Journal of Extracellular Vesicles

TECHNICAL NOTE OPEN ACCESS

Defining Biological Variability, Analytical Precision and Quantitative Biophysiochemical Characterization of Human Urinary Extracellular Vesicles

Edita Aksamitiene[1,2] | Jaena Park[1,2,3] | Marina Marjanovic[1,2] | Stephen A. Boppart[1,2,3,4,5,6,7]

[1]Beckman Institute for Advanced Science and Technology, University of Illinois Urbana-Champaign, Urbana, Illinois, USA | [2]NIH/NIBIB P41 Center for Label-Free Imaging and Multiscale Biophotonics, University of Illinois Urbana-Champaign, Urbana, Illinois, USA | [3]Department of Bioengineering, University of Illinois Urbana-Champaign, Urbana, Illinois, USA | [4]Department of Electrical and Computer Engineering, University of Illinois Urbana-Champaign, Urbana, Illinois, USA | [5]Cancer Center at Illinois, University of Illinois Urbana-Champaign, Urbana, Illinois, USA | [6]Carle Illinois College of Medicine, University of Illinois Urbana-Champaign, Urbana, Illinois, USA | [7]Interdisciplinary Health Sciences Institute, University of Illinois Urbana-Champaign, Urbana, Illinois, USA

Correspondence: Stephen A. Boppart (boppart@illinois.edu)

Received: 15 November 2024 | **Accepted:** 18 April 2025

Funding: This research was supported in part by grants from NIH/NIBIB (P41EB031772) and the Allen Distinguished Investigator Program, a Paul G. Allen Frontiers Group advised program of the Paul G. Allen Family Foundation.

Keywords: analytical precision | biological variability | biomarker quantitation | biophysiochemical properties | coefficient of variation | urinary extracellular vesicles | repeatability

ABSTRACT

The magnitude of combined analytical errors of urinary extracellular vesicle (uEV) preparation and measurement techniques (CV_A) has not been thoroughly investigated to determine whether it exceeds biological variations. We utilized technical replicates of human urine to assess the repeatability of uEV concentration and size measurements by nanoparticle tracking analysis (NTA) following differential velocity centrifugation (DC), silicon carbide, or polyethylene glycol uEV isolation methods. The DC method attained the highest precision. Consequently, DC-derived uEV size, most abundant protein levels, and optical redox ratio (ORR) were further assessed by dynamic light scattering (DLS), immunoblotting or multi-photon (SLAM) microscopy. Procedural errors primarily affected uEV counting and uEV-associated protein quantification, while instrumental errors contributed most to the total variability of NTA- and DLS-mediated uEV sizing processes. The intra-individual variability (CV_I) of uEV counts assessed by NTA was smaller than inter-individual variability (CV_G), resulting in an estimated index of individuality IOI < 0.6, suggesting that personalized reference interval (RI) is more suitable for interpretation of changes in subject's test results. Population-based RI was more appropriate for ORR (IOI > 1.4). The analytical performance of DC-NTA and DC-SLAM techniques met optimal $CV_A < 0.5 \times CV_I$ criteria, indicating their suitability for further testing in clinical laboratory settings.

Abbreviations: CA, cellulose acetate; CL, camera level; CT, (video data) capture time; CV, coefficient of variation; CV_A, analytical coefficient of variation; CV_{FA}, sample (final analyte) draw coefficient of variation; CV_G, inter-individual coefficient of variation; CV_I, intra-individual coefficient of variation; CV_{RR}, intra-day between-run coefficient of variation; CV_{TR}, procedural sample processing (EV isolation from technical replicates) coefficient of variation; CV_W, intra-day within-run coefficient of variation; DC, differential velocity centrifugation; DF, dilution factor; DLS, dynamic light scattering; DT, detection threshold; DTT, dithiothreitol; EV, extracellular vesicle; EXO, exosome; FA, final analyte; FOV, field of view; FRV, final reading value; HD, hydrodynamic diameter; IB, immunoblotting; IOI, index of individuality; MS, mass spectrometry; MSWB, Multi-strip Western Blotting; MV, microvesicle; NTA, nanoparticle tracking analysis; ORR, optical redox ratio; PA, primary (undiluted stock) analyte; PBS, phosphate buffered saline; PDI, polydispersity index; PEG, polyethylene glycol; PES, polyethersulfone; PPF, particles per frame; PT, pellet; PVDF, poly(vinylidene fluoride); RCV, relative change value; RI, reference interval; RM, repeated measurement; RR, replicate run; SEC, size exclusion chromatography; SiC, silicon carbide; SLAM, simultaneous label-free autofluorescence multi-harmonic; SN, supernatant; SPS, syringe pump speed; TR, technical replicate; UC, ultracentrifugation; UF, ultrafiltration; VCA, variance component analysis.

Edita Aksamitiene and Jaena Park contributed equally to this work.

1 | Introduction

The thorough design and repeatable execution of an experimental research study play crucial roles in ensuring both reliability and reproducibility of research findings. This is particularly important in pre-clinical exploration of candidate biomarker substances found in accessible, non-invasive or minimally invasive liquid biopsies, including blood, saliva, cerebrospinal fluid, breast milk and urine (Lone et al. 2022). One such emerging analyte is extracellular vesicles (EVs), which are formed by the direct shedding or budding of cellular plasma membrane or through the endosomal exocytosis pathway. Containing an enclosed cargo of versatile biomolecules, EVs exert evolutionary conserved intercellular communication roles that impact fundamental biological processes (Lee et al. 2012). Furthermore, these biostable, bioactive, biocompatible and ubiquitous micro- and nano-scale particles have demonstrated promising potential as predictive, diagnostic or prognostic biomarkers. Analysis of EVs can reveal information relevant to assessing the risk of developing cancer, detecting early cancer onset, or assessing the risk of tumor progression in response to specific therapies (Kalluri and McAndrews 2023; Yang et al. 2023; Palacios-Ferrer et al. 2021; Testa et al. 2021; Lee et al. 2022; Yu et al. 2022; Sohal and Kasinski 2023; Clos-Garcia et al. 2018; Royo et al. 2016; Lai et al. 2022). Moreover, the appropriately tailored autologous EVs may be employed as nanocarriers for loaded therapeutic anti-cancer drugs (Sidhom et al. 2020; Gao et al. 2022).

Analytical samples enriched with different EV sub-populations can be obtained by various sedimentation, precipitation, sieving/trapping, sorting, size-exclusion and other techniques (Lai et al. 2022; Gupta et al. 2018; Sidhom et al. 2020; Gao et al. 2022; Liu et al. 2022; Yakubovich et al. 2022; Singh et al. 2023; Xu et al. 2016); including differential velocity centrifugation (DC) (which typically incorporates ultracentrifugation (UC) step performed at very large g forces) and hydrophilic nanoporous silicon carbide (SiC) sorbent- or polyethylene glycol (PEG) polymer-based methods (Liu et al. 2022; Yakubovich et al. 2022; Singh et al. 2023; Haj-Ahmad 2018). While in most research applications, the isolated particles are lysed and used for proteomic, transcriptomic or metabolomic analyzes of their content, a reserved portion of intact EV suspension may be set aside for a relatively rapid 'point-of-care' determination of biophysicochemical measurands, such as concentration, size, charge and/or intrinsic metabolic activity. The latter is partially reflected by optical redox ratio (ORR) measuring the balance between two key intracellular coenzyme molecules: reduced nicotinamide adenine dinucleotide (NAD(P)H) and oxidized flavin adenine dinucleotide (FAD) (Stankovic and DiLauri 2008). This is due to the recognition that, apart from the differential changes in their cargo, some EV sub-populations appear to be more abundant or are altered in patients with certain types of cancer (Yu et al. 2022; Clos-Garcia et al. 2018; Royo et al. 2016; Lai et al. 2022; Gupta et al. 2018).

If any quantitative EV property measurement result is expected to serve as a basis for appropriate treatment dose selection or critical clinical care decisions, it is essential to identify and acknowledge potential sources of error as well as assess the magnitude of experimental variability in EV analysis workflow to ensure that variations in results are acceptable. Therefore, evaluation of precision is a critical part of any method validation process (Figure 1). Random errors may occur around the time of (a) biological sample collection, handling, storage and initial preparation steps (pre-analytical imprecision), (b) sample processing for analyte extraction and measurement (peri-analytical imprecision) or (c) data analysis (post-analytical imprecision) (Erdbrugger et al. 2021). *Short-term precision* refers to the ability of a method to generate consistent results under *repeatability* conditions where the same analyst/operator conducts a series of independent successive measurements using the same instrumental system/method/assay on identical test items or subjects within the same laboratory over a short period of time to quantify the same measurand of interest. By contrast, *intermediate precision* is evaluated over extended time intervals (e.g., days, months), albeit with minimal changes in raw materials or reagents used to generate the test items, whereas *reproducibility* is assessed at different laboratory level (Analytical Methods Committee Amctb N 2015; Plant and Hanisch 2020) (Figure 1A). The extent of relative variability can be expressed as the *coefficient of variation* (CV). A lower CV value indicates that the data points are more consistent, reflecting lower uncertainty in the measurements. Conversely, a higher CV indicates greater data dispersion around the mean, leading to increased uncertainty and lower repeatability, reproducibility, or intermediate precision. A glossary of basic metrological concepts and key terms used in this study is provided in the Supplementary Material (see Supplemental Text and Supplemental Tables).

Despite clear clinical potential of biofluid-derived EVs, little is known about the *cumulative precision* of their isolation and characterisation techniques. For instance, potentially clinically-relevant properties of urinary EVs (uEVs) can be assessed by nanoparticle tracking analysis (NTA) (Kurian et al. 2021, Comfort et al., 2021), dynamic light scattering (DLS) (Lai et al. 2022, Kurian et al. 2021), conventional or higher-throughput comparative Western Blotting (Taylor et al. 2022; Kowal et al. 2017; Aksamitiene et al. 2007) or simultaneous label-free autofluorescence multiharmonic (SLAM) microscopy (Boppart et al. 2019; Sorrells et al. 2024), however, the *combined uncertainties* of data yielded from these techniques following specific uEV isolation methods have not been thoroughly investigated to determine if they exceed natural biological variability. Without a priori knowledge of statistical biological and technical variation of well-established (clinical) or candidate (pre-clinical) analytes and their homeostatic set points in healthy humans, making clinical decisions regarding the pathological condition(s) is nearly impossible (Braga and Panteghini 2016). Hence, following the recommendations of the Urine Task Force of the Rigor and Standardization Subcommittee of the International Society for Extracellular Vesicles (ISEV) (Erdbrugger et al. 2021), we sought to evaluate the peri-analytical precision of three relatively inexpensive, moderately rapid, high yield-producing uEV isolation methods: (1) sequential centrifugation at increasing speeds (DC/UC), (2) PEG-based precipitation or (3) SiC-based adsorbtion–desorbtion reaction used to pellet uEVs. After identifying the most precise uEV isolation procedure, we aimed to fit a hierarchical, fully nested random factor analysis of variance model to discern the contribution of additional sources of variance to the overall analytical variability of uEV concentration, size, most abundant protein content or ORR measurement processes (CV_A) (Figure 1B). This was followed by exploring strategies to eliminate the most influential variance components if any were identified. Our last objective was to assess the

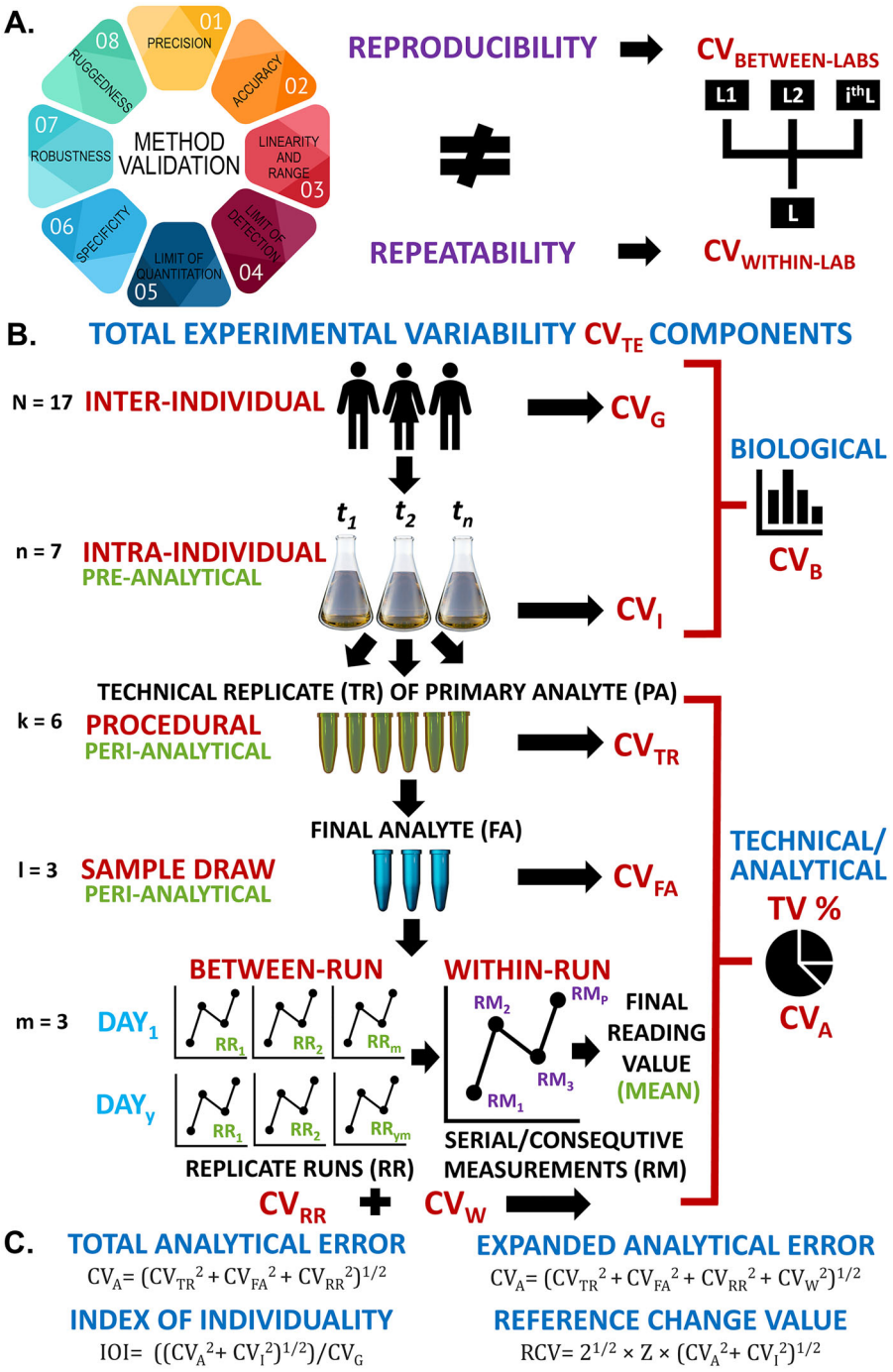

FIGURE 1 | Study design and concepts. (A) Assessment of precision expressed as coefficient of variation percentage (CV%) is a part of the standard method validation process. Repeatability (short-term precision), which tests the variability in repeated measurements on the same item under the same conditions—same operator, instrument, method, laboratory and over a short timeframe (often minutes to hours) is not equal to reproducibility (long-term precision), which tests the consistency of data obtained at different laboratories/sites. (B) An experimental design for evaluation of the total experimental variability (CV_{TE}) of biophysical biofluid-derived extracellular vesicle (EV) property assessment. Biological inter-individual (CV_G) and intra-individual (CV_I) variations are part of natural physiological fluctuations and inherent genetic/environmental differences in the analyte of interest. Variations in the procedural isolation of primary analyte (PA) (estimated by CV_{TR}), pipetting/sample draw (CV_{FA}), and instrumental sample read (between-run (CV_{RR}) and within-run (CV_W)) are main sources of gross technical/analytical error (CV_A). In this study, the *short-term intra-laboratory precision* was assessed when multiple EV-enriched PAs were prepared from k number of technical replicates (TRs), that is, multiple sub-samples of one biological sample (urine) collected at the defined time of day by one selected EV isolation method of choice. These were further consecutively sampled and aliquoted for l number of times to prepare appropriately diluted final analytes (FA) suitable for downstream analysis. For each FA sample, m number of replicate runs (RRs) were carried out on the same day to measure the concentration, size or optical redox ratio (ORR) of either small or large urinary EVs (uEVs). Each RR consisted of p number of serial repeated measurements (RMs). Their values were averaged at the end of data capture cycle to yield one final reading value (FRV), which is mean. *Intermediate precision* is typically evaluated on stable samples that would be analyzed by m number of RRs on y number of different days. (C) Uncertainties were combined using the square root of the sum of squares method, commonly referred to as combining

uncertainties in quadrature. A nested random factor ANOVA was applied to partition the total variance (TV) into individual variance components and to estimate the relative contribution of each hierarchical factor (TR, FA, RR with/without RM) to the overall measurement precision. Calculating both biological (CV_B) and analytical (CV_A) variability of the analyte of interest in healthy individuals is critical for establishing the reference change value (RCV) and the index of individuality (IOI). If the change in a patient's clinical test results exceeds the RCV, it suggests a significant alteration beyond normal fluctuations. IOI is used to determine the most appropriate use of either personalized or population-based reference intervals (RIs).

inherent biological intra-individual (CV_I) and inter-individual (CV_G) variability of principal uEV measurands in a limited cohort of healthy individuals. CV_I and CV_G are crucial for determining the index of individuality (IOI) (Braga and Panteghini 2016). IOI helps decide whether population- or individual-based reference intervals (RI) (a range of values that is considered normal for a healthy person) are more appropriate for evaluating the changes in an analyte compared to the baseline, as measured by the relative change value (RCV) at either 95% or 99% confidence levels (Walton 2012) (Figure 1C). With a sufficient wash-out period, the homeostatic point for personalized RI can be calculated from as few as three longitudinal measurements (Walton 2012; Coskun et al. 2021; Petersen et al. 1999; Schork 2022), but accurate RI calculation requires inclusive CV_A (Jones and Barker 2008), which we aimed at estimating in this non-clinical metrological feasibility study.

2 | Materials and Methods

2.1 | Ethics Statement

All research procedures involving enrolled human adult participants have been carried out in accordance with The Code of Ethics of the World Medical Association (Declaration of Helsinki 1964) and were approved by the Institutional Review Board of University of Illinois Urbana-Champaign (#19281) or Carle Foundation Hospital (#18CCC1708) (Urbana, IL). Written informed consent was obtained from all individuals.

2.2 | Chemical Reagents and Labware

Chemicals used in the study met or exceeded the purity standard set by the American Chemical Society (ACS). uEV resuspension buffer (PBS-TR) consisted of Ca^{2+}/Mg^{2+}-free phosphate buffered saline (PBS) (pH 7.0) (Cytiva, Marlborough, MA, #SH30256.01) supplemented with 25 mM of ≥99% anhydrous D(+)-Trehalose (Chem-Impex Int., Wood Dale, IL, #31116), which was added to minimise the risk of EV aggregation during the short-term storage on ice or at 4°C (Bosch et al., 2016). PBS-TR was passed through 0.05 µm pore-size polyethersulfone (PES) syringe filter (Tisch Scientific, Cleves, OH, #SF18256) and stored at 4°C. To minimise the risk of particle loss due to adherence to the plastic, ultra-low protein binding tubes and ultra-low retention pipette tips were used.

2.3 | Pre-Analytical Conditions

There are numerous factors introducing unwanted pre-analytical variations in the urine specimen testing (Stankovic and DiLauri 2008). While some data shows no evidence of significant effect of source (raw) sample pre-processing or storage time on uEV number or size (Lee et al. 2023), their influence on metabolic status of uEVs remains unknown. Consequently, all particles in this study were isolated from raw (unfiltered), pristine (fresh, non-frozen) and naïve (chemically untreated) urine. First-morning voided mid-stream urine was collected from 7 healthy male (mean age = 43 years) and 10 healthy female (mean age = 35 years) adults (N = 17). For the evaluation of inter-individual (CV_G) and intra-individual (CV_I) biological variability of principle uEV measurands, on average 60 mL of urine was gathered into sterile 120 mL polypropylene specimen containers (TFS, #16-320-730). To evaluate diurnal variations, urine was collected at a specified time of the day (morning [6–9 AM], afternoon [noon to 3 PM], or evening [6–9 PM]). To assess the combined peri-analytical precision (CV_A), at least 252 mL of urine from single individual was collected in sterile 500 mL glass container, that is, a volume sufficient to be sub-divided into six or more equal portions, referred to as technical replicates (TRs). Only if total urine volume was lower than 42 mL, it was adjusted by adding PBS, but in general the urine to PBS ratio did not exceed a dilution factor (DF) value of 1.35. During specimen transportation, all containers were kept in a prechilled cooler. Upon arrival, urine was kept at 4°C and processed within 1 h of receipt following urinalysis. The pH, glucose, ketones, uromodulin, bilirubin, blood, protein, leukocyte, and nitrite levels were measured by Siemens CLINITEK Status+ Urine Analyzer using 1 mL urine aliquot dispensed onto a Siemens 2161 Multistix 10 SG Reagent Strip sensor.

2.4 | Peri-Analytical Sample Preparation Conditions

In each independent experiment conducted on a different day, all TRs generated from a unique biological specimen were processed simultaneously by one randomly chosen uEV isolation method. For all methods, urine was pre-clarified by sequential centrifugation at 800 × g for 10 min and then at 2000 × g for 30 min at 4°C to remove residual cells, debris and large particle contaminants. Negative control consisted of PBS alone processed in the same way as uEV samples. Since filtering a source sample before nanoparticle isolation might eliminate uEV subpopulations carrying a significant diagnostic or prognostic weight, any potential effects of filtration on final uEV counts, size and other properties were evaluated on the readily isolated uEV material.

2.4.1 | Urinary Extracellular Vesicle (uEV) Isolation by Differential Velocity Centrifugation (DC)

Pre-cleared urine was dispensed into six 36 mL thin-walled polyallomer tubes (TFS, #03141). Crude fraction of large size uEVs

designated as urinary microvesicles (uMVs) was isolated from 34 mL of pre-clarified urine by centrifugation at 12,000 × *g* for 1 h at 4°C using Sorvall WX+ series ultracentrifuge equipped with a 90° angle SureSpin 360 swinging-bucket rotor (TFS, #79368; Max speed: 30,000 rpm, 166 mm radius, K factor = 219). Acceleration and deceleration were set at level 9. Subsequently, 33 mL of supernatant (SN) was transferred into a new tube that was spun at 100,000 × *g* for 1 h at 4°C to separate medium-to-small size uEVs, referred to as exosomes (uEXO). The remaining SN was discarded, and the resulting 12K uMV or 100K uEXO pellets were resuspended in 55 or 100 µL of PBS-TR buffer, respectively (Figure 2). For some downstream analyzes, each resulting uMV or uEXO stock solution, referred to as primary analyte (PA), was further mixed with 0.05 µm pre-filtered PBS at a specified ratio to prepare a diluted working solution, referred to as the final analyte (FA). To reduce pipetting errors, 5 µL was set as a limit for dispensing viscous and concentrated PA samples. A resultant FA with DF = 400 was used to generate other more diluted FA suspensions.

2.4.2 | uEV Isolation Using Silicon Carbide (SiC) Matrix

SiC slurry was prepared by resuspending 6.25 g of 2000 grit size SiC powder (TedPella, #815-74) in 10 mL PBS. Three mL of SiC slurry was added to each 30 mL of urine following the pH adjustment to 8.6 using 1 M Tris (pH 11.0). At this specific pH, EVs are absorbed by the porous, negatively charged SiC sorbent matrix, while larger particles like proteins or ribosomes, which differ in their isoelectric points, are excluded. After 1 h incubation at RT on a rotator revolving at 26 rpm, the mixture was centrifuged at 545 × *g* for 5 min at 24°C. The SN was discarded and sorbent-bound uEVs were eluted in 3 mL PBS (pH 6.0) for 0.5 h at RT while rotating the tubes. After 25 × *g* spin for 5 min, the SN was loaded into a 3 mL Luer-Lok glass syringe and filtered by gravity through the pre-moistened 1 µm PES filter with a gentle push of the plunger at the end (Figure 2). All PAs were stored at 4°C and analyzed within 2 h.

2.4.3 | Polyethylene Glycol (PEG)-Based uEV Isolation

Twenty grams (20 g) of PEG-8000 polymer (Post Apple Scientific, North East, PA) was dissolved in 50 mL of 0.05 µL pre-filtered PBS to yield 40% w/v stock PEG solution. After 15 min heating at 37°C, the solution was sterilised via 1 µm PES filter (Millipore-Sigma, #WHA68842510) and stored at RT. Each 5 mL of pre-cleared urine was mixed with 1 mL stock PEG solution followed by an incubation on a rotating platform for 24 h at 4°C. Co-precipitated uEV-PEG complexes were sedimented at 1500 × *g* for 30 min and resuspended in 200 µL PBS-TR. For downstream analysis, 40 µL of PA was diluted in a final 2 mL volume to prepare a FA (DF = 50), which was passed through the DNAse/RNase free Spin-X 0.45 µm cellulose acetate (CA) centrifuge tube filter (Corning Inc., Corning, NY, #8163) using benchtop mySPIN 6 Mini Centrifuge (TFS, #75004061) for 3 min at RT and max speed (Figure 2). Further dilutions of spin-filtered FAs were prepared in 0.05 µm pre-filtered PBS as needed.

2.5 | Peri-Analytical Sample Measurement Conditions

The mid-term and long-term sample storage at 4°C, −20°C or −80°C as well as freeze-thaw cycles of isolated EV suspensions are known to significantly impact their counts (Görgens et al. 2022). Therefore, all isolated uEVs in this study were kept at 4°C and, depending on the type of analytical downstream technique, were either analyzed within the same day or were immediately lysed and stored at −20°C. The undiluted PA samples awaiting analysis were kept on ice. To minimise the risk of vesicle aggregation, FA samples were prepared immediately prior to their analysis. Samples were profiled individually, and all measurements were analyzed in the order they were taken.

2.5.1 | Transmission Electron Microscopy (TEM)

For DC-derived uEV morphology assessment by TEM, the PAs were prepared as described in Section 2.4.1. For TEM analysis of uEVs isolated by the SiC method, three TRs of 30 mL of pre-clarified urine were incubated with SiC slurry for 1 h at RT. uEVs were eluted in 6 mL PBS (pH = 6.0). The eluates were combined and topped with an additional 16 mL PBS (pH = 7.0) followed by centrifugation at 100,000 × *g* for 1 h at 4°C. uEV pellets were resuspended in 60 µL PBS-TR. For TEM of PEG-derived uEV samples, 25 mL of pre-clarified urine was incubated with 5 mL of stock PEG solution for 12 h at 4°C. uEVs were sedimented at 1500 × *g* for 30 min and resuspended in 100 µL of PBS-TR. One drop (~20 µL) of EVs was adsorbed to a 200-mesh carbon-stabilized Formvar-covered copper grid (Ted Pella, #01811) and incubated for 3 min at RT upside down. The excess solution was removed using filter paper, and the grid was negatively stained with 2% w/v uranyl acetate. Images of stabilized EVs were taken with the FEI Tecnai G2 F20 X-TWIN transmission electron microscope equipped with 120 kV electron detector and AMT 4k×4k CMOS camera. Images were captured and analyzed in AMT Capture Engine Software v. 7.0.1.

2.5.2 | Fluorescence Microscopy

A volume of 100 µL of isolated uEV suspension or 100 µL of PBS-TR (negative control) were labelled with 1 µL of 1 mM cell-permeant SYTO RNASelect nucleic acid stain (absorption/emission maxima ~490/530 nm) for 30 min at 37°C (TFS, # S32703). When bound to RNA inside the vesicles, this dye produces bright green-fluorescent signal. The images of labelled uEVs spread onto a 35 mm imaging dish with #0 glass coverslip (MatTek, Ashland, MA, #P35G-0-20-C) were taken by inverted Zeiss Axio Observer D1 microscope using a 63x oil objective and green-fluorescence FITC filter.

2.5.3 | Immunoblotting (IB)

Undiluted primary analyte (PA) samples containing freshly isolated uEVs were lysed in ice-cold 2× lysis buffer (100 mM HEPES (pH 7.4), 300 mM NaCl, 2% Triton X-100, 2 mM EGTA, 20% Glycerol, 1% sodium deoxycholate and 0.2% SDS)

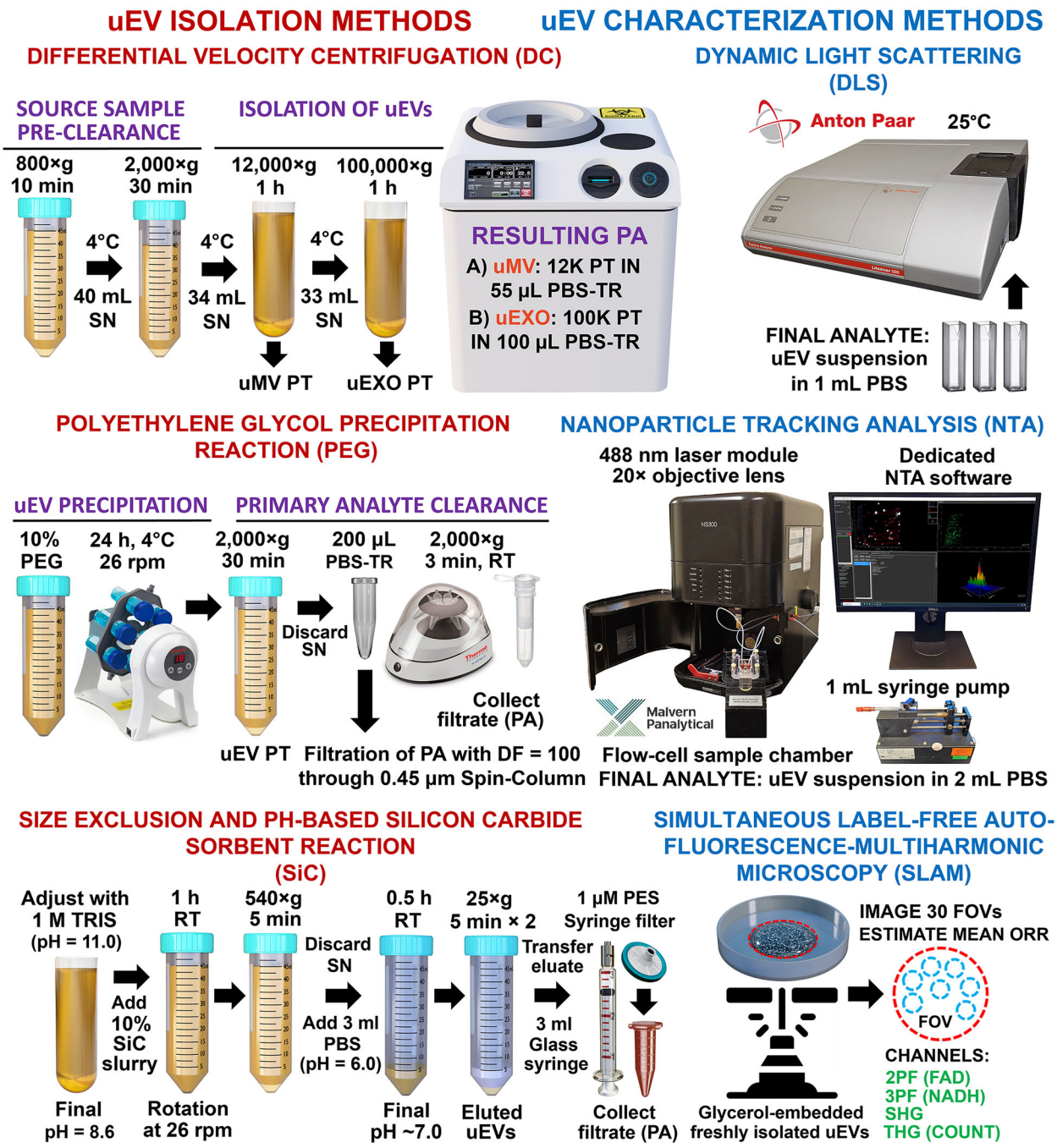

FIGURE 2 | Urinary extracellular vesicle (uEV) isolation and characterisation methods used in this study. uEVs isolated by differential velocity centrifugation (DC), polyethylene glycol (PEG) co-precipitation or silicon carbide (SiC) sorbent pH-sensitive binding-based methods (right panel) were characterised by the dynamic light scattering (DLS), nanoparticle tracking analysis (NTA), or inverted simultaneous label-free autofluorescence multi-harmonic (SLAM) microscopy techniques (left panel) that measured average uEV particle size (hydrodynamic diameter), polydispersity index (PDI), concentration and metabolic activity (ORR computed from FAD/(NADH+FAD) formula) either in liquid or semi-solid phase samples, respectively. 2PF = two-photon autofluorescence, 3PF = three-photon autofluorescence, FA = final analyte, FOV = field of view, ORR = optical redox ratio, PBS = phosphate-buffered saline, PBS-TR = phosphate buffered saline and trehalose buffer, PT = pellet, RT = room temperature, SHG = second-harmonic generation, SN = supernatant, THG = third-harmonic generation.

supplemented with protease (A.G. Scientific, San Diego, CA, #P-1512) and phosphatase inhibitor (Millipore-Sigma, #4693159001) cocktails at a 1:1 ratio. Total protein of lysed or intact uEV samples and/or EV-depleted urine was determined by BCA assay. After LDS-PAGE and comparative higher-throughput Multi-Strip Western Blotting, where each membrane was subdivided into several horizontal strips containing a migratory region for the protein of interest as described previously (Fey et al. 2017), the resulting aligned multistrip blots were probed with anti-ALIX (BosterBio, Pleasanton, CA, #M01751), anti-TSG101 (BosterBio, #M01233), anti-CD9 (BosterBio, #M01202), anti-GM130 GOLGA2 (BosterBio, #M05865), anti-PDI (clone C81H6), anti-pyruvate

dehydrogenase (clone C54G1), anti-VDAC, anti-COX IV (clone 3E11), anti-PKM1/2 (clone C103A3), anti-GAPDH (D16H11) XP (Cell Signaling Technology, Danvers, MA, #3501, #3205, #4866, #4850, #3190, and #5174, respectively) rabbit monoclonal antibodies, anti-Flotillin 1 (Clone 18) (BD Biosciences, # 610820) mouse monoclonal antibodies or anti-Tamm-Horsfall protein (THP, Antibodies.com, #A30469) rabbit polyclonal antibodies. Protein bands were visualized after 5 min reaction with a working chemiluminescent substrate reagent solution (TFS, #34580). Total protein was assessed by Coomassie G-250-based SimplyBlue gel stain for 24 h at RT (TFS, #LC6060). Chemiluminescent or colorimetric signals emitted from reactive protein bands were captured by a ChemiDoc MP Imaging System (BioRad, Hercules, CA) and analyzed in GelAnalyzer v.23.1 software.

2.5.4 | Nanoparticle Tracking Analysis

A NanoSight NS300 apparatus (Malvern Panalytical, Malvern, UK) operating at controlled room temperature conditions and equipped with syringe pump device was used to analyze the mean number-weighted size, modal size, and concentration of freshly isolated uEV particles that were resuspended in a final 2 mL volume providing an optimal particle density ranging between 40 and 80 particles per frame (PPF) or as indicated in the text (Figure 2). The video data of particle flow was acquired using camera sensitivity level (CL) set to 13 for uMV and to 14 for uEXO fractions. uEVs isolated by the SiC or PEG methods were analyzed at CL set to either 14 or 15. The syringe pump speed (SPS) controlling the flow rate of the sample was set to 35. Video data capture time (CT) was set to either 30 or 60 s to collect seven intra-sample repeated measurement (RM) data points.

Each *final analyte* (FA) was measured either once or multiple times if serial *replicate run* (RR) analysis was carried out by a single operator over a relatively short period of time within 1 day. Prior to delivery of a new sample bolus into disposable 1 mL syringe (Air-Tite Products Co., Inc., Virginia Beach, VA), equipment underwent a partial 'reset' procedure: a flow cell and tubing were thoroughly washed by at least three flushes with appropriate diluent buffer to remove any residual material from a previous sample. Additionally, the tubing was aerated with 5–10 air passes. The *runs* were considered *matched* if they analyzed uEVs originating from the same person and were performed on different days or at different times of the same day (e.g., morning, afternoon and evening). *Independent runs* used uEVs originating from different individuals. Prior to each matched or independent run, the flow cell was fully disassembled, sanitised and cleaned. The instrument was routinely calibrated using 100 nm NIST-traceable polystyrene latex nanospheres with a target reference concentration of 1×10^9 particles/mL (TFS, #3100A). Valid particle track number was determined at detection threshold (DT) levels set to either 3 or 5. The DF was recorded during each run session to enable an automated particle concentration upgrade by the NTA v.3.4.4 software with a result expressed as particles/mL of PA. The last video recording was used to replace any outlying RM value detected by the Grubbs test at the 95% confidence level. In the absence of significant outliers, it replaced one RM with the minimum concentration and associated mean/modal size value; otherwise, it was discarded. The resultant six RM data points were averaged to obtain one final reading value (FRV)—the main outcome of NTA run. Where applicable, particle concentration results were normalized and expressed as particles/mL of raw urine. To express the concentration of uEVs relative to the original volume of raw urine, the following equation was applied: (DF-adjusted concentration of EVs in PA × PA resuspension volume)/(Volume of source raw urine processed). This normalization enabled consistent comparison of uEV concentrations between samples by adjusting for differences in initial urine volume and processing conditions.

2.5.5 | Dynamic Light Scattering

The hydrodynamic diameter (HD), polydispersity index (PDI) and intensity-, number- or volume-weighted distribution of uEV particle size (IW, NW and VW) were measured by Anton-Paar Litesizer 500 particle analyzer equipped with 658 nm 40 mW semiconductor laser diode (Figure 2). For DLS analysis, isolated uEVs were resuspended in a final 1 mL PBS volume in a disposable polystyrene cuvette (Sarstedt, #67.745). After achieving thermal equilibrium of an instrument at 25°C, ten 30-second-long *repeated* intra-sample *measurements* (RMs) were recorded at a 90° side-scatter measurement angle and an automatic focus position. A manually fixed focus position was used for the subsequent serial data capture. Data was analyzed by Anton-Paar Kalliope Professional Software v.2.16.0 using 'General Analysis' model and 'Advanced' cumulant model settings, with 'Material' parameter set to 'Protein'. The expected PDI of monodisperse and homogeneous samples was empirically set to ≤10%. The PDI of polydisperse samples with a larger variation in particle size was expected to fall between 10% and 40%, whereas the samples with aggregated or agglomerated particles or large-size contaminants were expected to have a PDI > 40%. The performance of DLS instrument was routinely tested using 100 nm NIST-traceable latex beads (TFS, #3100A).

2.5.6 | Simultaneous Label-Free Autofluorescence Multiharmonic (SLAM) Microscopy

To prepare the FAs for SLAM, 10 μL of each PA or PBS (negative control) was mixed with 40 μL of pre-chilled glycerol (Sigma-Aldrich, # G5516). Embedded uEVs were dispensed on a #2 thickness (0.19–0.25 mm) cover glass (Ted Pella, Redding, CA, #260454). The imaging plane was set at 50 μm above the cover glass. Pixel dwell time was 50 μs, resulting in 8 s acquisition time per FOV with a frame size of 200 μm × 200 μm (400×400 pixels). Four sequential sets of long-pass dichroic mirrors and bandpass filters of 365–375, 420–480, 540–570 and 580–640 nm were used to separate the collected signals into the third-harmonic generation (THG), three-photon autofluorescence (3PF), second-harmonic generation (SHG) and two-photon autofluorescence (2PF) channels as described previously (You et al. 2018) (Figure 2). The intensities of signals were normalized to the laser power output measured at the sample plane at different days of sample imaging. uEV segmentation by morphological features was performed using the pre-defined THG signal threshold (Park et al. 2022). The standardised mask was then applied to other channels, and the intensity of 3PF signal emitted from individual particles was

divided by the sum of 2PF and 3PF signals to derive the ORR based on ORR = FAD / (NAD(P)H + FAD) formula as described previously (Park et al. 2022; Quinn et al. 2013; Lim et al. 2022). Unless indicated otherwise, individual ORR values were averaged per 25 random FOVs. Five additional FOVs were recorded to replace any two outlying FOV data points as detected by Grubbs test at 95% confidence level (first-pass) or 99% confidence level (second-pass). In separate cases, where the same FOV was imaged repetitively, data analysis engaged manual single particle tracking algorithm. Routine SLAM signal quality check involved quantifying the NAD(P)H or FAD autofluorescence in freshly prepared 10 mM NADH or 1 mM FAD (Millipore-Sigma, #481913 and #F6625) solutions, which exhibited maximum fluorescence spectra at 460 and 535 nm, respectively. Linear dependence of the fluorescence signal intensity on the concentration of NADH or FAD mixtures prepared in various buffers was described elsewhere (Lim et al. 2022).

2.6 | Statistical Data Analysis

Descriptive statistical data analysis and data visualization was conducted using GraphPad v. 9.5.1 software. In plots, the arithmetic mean was depicted either with standard deviation (SD), standard error (SE) or 95% confidence interval (CI) error bars. The median was displayed without error bars. Data sets were assessed for normality using the Shapiro–Wilk test. Two-tailed paired or unpaired Student's *t*-tests were used to determine the significance of bidirectional changes between two data groups. One-way ANOVA with post-hoc Tukey HSD test was employed to assess the significance of difference among three or more groups at $\alpha = 0.05$. The degree of data dispersion was expressed as coefficient of variation (CV) percentage, which was calculated as an absolute value of SD of measurements multiplied by 100 and divided by the sample mean. To estimate average CV across two or more independent groups of data, the pooled SD (weighted average of the SDs of the data groups) was divided by the grand mean of all data groups. The biological and analytical variability of different uEV measurands was estimated by a single experienced operator within a single laboratory, after a preliminary assessment of operator-to-operator agreement (Figure 1A).

To avoid issues with linear interpolation when attempting to restore the balanced design for ANOVA, the responses recorded over five additional FOVs in SLAM microscopy or over two additional RRs in DLS or NTA datasets were used to replace any two outlying FRVs. Outliers typically exceeded $\pm 3 \times$ SD of the mean or $\pm 1.5 \times$ IQR (interquartile range) of the median and were detected by a two-sided Grubbs test, which compared the *G* test statistic to the G critical value at either a 95% confidence level (for groups of RMs) or a 99% confidence level (for groups of RRs or TRs) for the minimum and maximum responses. In the absence of outliers, these additionally collected variables were omitted from the final data analysis.

Variance component analysis (VCA) was conducted using MiniTab v. 21.3.1 software or Real-Statistics Resource Pack MS Excel add-in to assess the relative impact of procedural (TR sample processing, CV_{TR}), sample draw (FA preparation, CV_{FA}), as well as instrumental read (within-run (CV_W) and between-run (CV_B)) sources of error to the total observed variability of entire uEV isolation and analysis process (Figure 1B). Expected mean square (EMS) values for each factor level were used to derive corresponding SD and CV% values. The sum of EMS values was used to estimate the total variance (TV). The proportional percentage contribution of different variance components to the TV of uEV measurement process, which was set to 100%, was visualized using pie charts. Specifically, a fully nested random effects ANOVA model $Y_{klm} = \mu + r_k + r_{kl} + \varepsilon_{klm,}$ where μ represents (grand) mean response, r denotes a random effect, ε is random error, k is technical replicate (TR), l is final analyte (FA) within the TR, and m signifies replicate run (RR) within the FA and TR, was fitted to ascribe variance components at each factor level for the NTA and DLS measurements. No interaction was included in this model since factors were not crossed. Combined peri-analytical precision, expressed as CV_A percentage, was calculated as $CV_A = (CV_{TR}^2 + CV_{FA}^2 + CV_{RR}^2)^{1/2}$. In case of applied extended nested ANOVA model $Y_{klmp} = \mu + r_k + r_{kl} + r_{klm} + \varepsilon_{klmp}$, where p is repeated measurements (RMs) nested within RR, FA and TR, the extended formula $CV_A = (CV_{TR}^2 + CV_{FA}^2 + CV_{RR}^2 + CV_{RM}^2)^{1/2}$ included random within-run variations $CV_W = CV_{RM}$.

For SLAM microscopy, the EMS, SD, CV% and TV% values for between-group and within-group sources of variance were derived from one-way random factor ANOVA model $Y_{kl} = \mu + r_k + \varepsilon_{kl}$, where k is TR and l is FA (random error). Combined analytical precision was expressed as $CV_A = (CV_{TR}^2 + CV_{FA}^2)^{1/2}$. In the expanded nested ANOVA model $Y_{klm} = \mu + r_k + r_{kl} + \varepsilon_{klm}$, where m is FOV (image frames) nested within FA and TR, intra-sample variations were defined as CV_W, and combined analytical precision was calculated as $CV_A = (CV_{TR}^2 + CV_{FA}^2 + CV_W^2)^{1/2}$.

Biological inter-individual variability (CV_G) and intra-individual variability (CV_I) were estimated by characterising uEVs from samples repeatedly collected from different individuals or from the same individuals under similar conditions, respectively. *Optimal, desired, and minimal analytical method performance goals* were set as $CV_A = 0.25 \times CV_I$, $CV_A = 0.5 \times CV_I$ or $CV_A = 0.75 \times CV_I$, respectively (Sikaris 2008). Reference change value (RCV) for each measurand was estimated by $RCV = 2^{1/2} \times Z \times ((CV_A^2 + CV_I^2)^{1/2})$ formula, where Z-score equaled either to 1.96 for $p < 0.05$ or 2.58 for $p < 0.01$ for bidirectional (two-sided) measurement value change scenario, or to 1.64 for $p < 0.05$ or 2.33 for $p < 0.01$ in unidirectional (one-sided) change scenario. Index of individuality (IOI) was calculated as $IOI = ((CV_A^2 + CV_I^2)^{1/2}) / CV_G$ as shown in Figure 1C. An IOI below 0.6 indicate that the individual's measurements are more consistent relative to the population variability, suggesting that individual-based reference intervals (RIs) are more appropriate, whereas an IOI above 1.4 favors population-based RI (Fraser and Harris 1989; Sithiravel et al. 2022).

3 | Results

3.1 | Validation of Isolated uEV Purity and Abundance

The purity, composition, and structural integrity of uEVs was assessed by several ancillary techniques (Figure 3). Representative high magnification TEM images indicated that uEV populations produced by DC, SiC or PEG methods had minimal

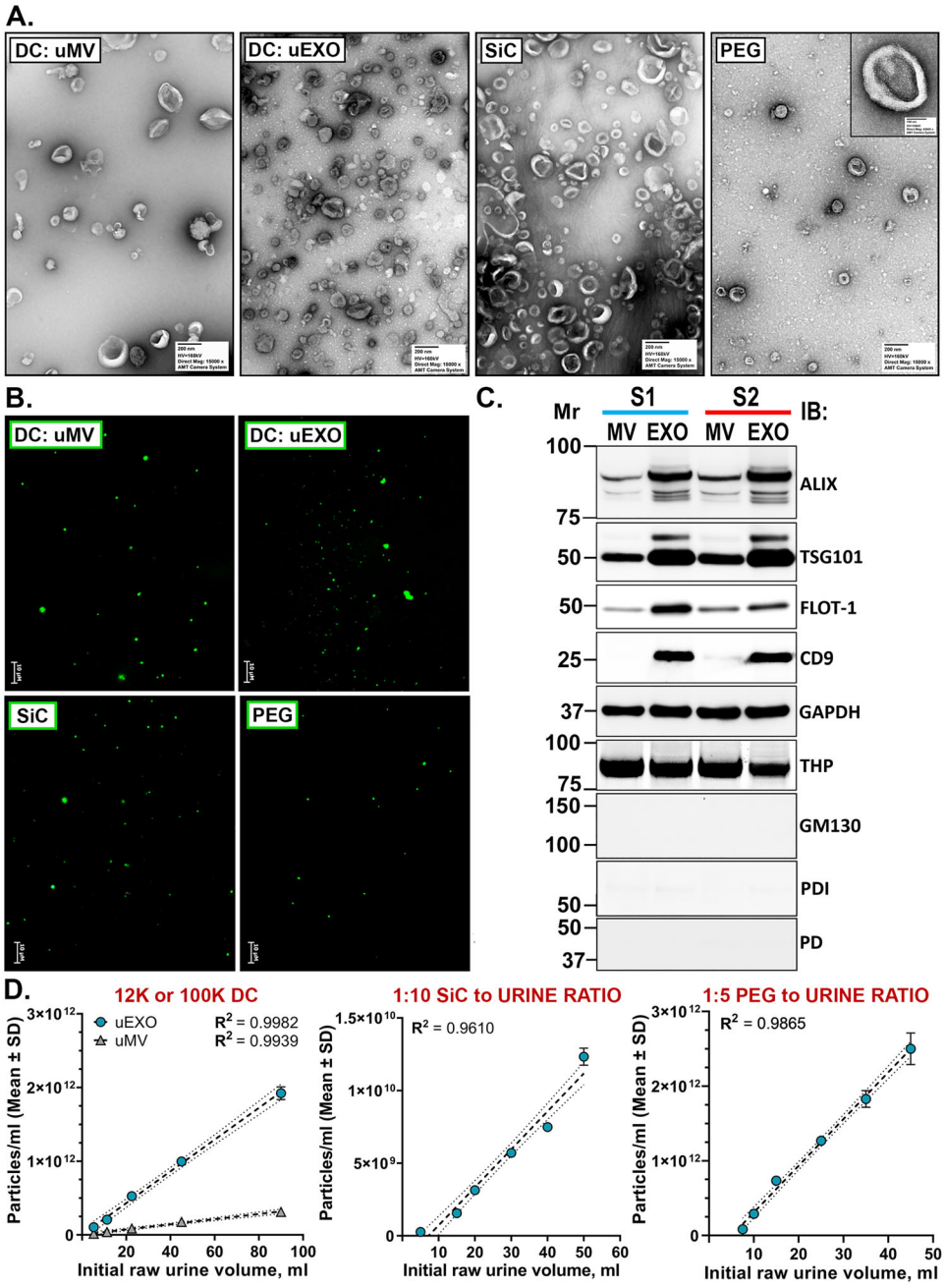

FIGURE 3 | A-C. Prove of urinary extracellular vesicle (uEV) particle existence in the primary analyte samples derived by different uEV isolation methods by ancillary transmission electron microscopy (TEM) (A), fluorescence microscopy (FM) (B) and Western Blotting/Immunoblotting (IB) (C) methods. TEM shows a typical cup-shape EV morphology (EV drying artefact) at 3200 ms exposure and either medium 15,000× (bar size = 200 nm) or high 43,000× (bar size = 100 nm, inlet image) magnification; IB shows known EV protein biomarker expression such as Alix, TSG101, Flotillin-1, CD-9 and PKM1/2 in different subject (S1, S2) uEV samples that are free of Golgi, endoplasmic reticulum or mitochondria organelle contaminants as indicated by the absence of GM130, protein disulfide isomerase (PDI) or pyruvate dehydrogenase (PD) proteins; FM displays green fluorescent signal emitted from SYTO RNASelect-stained internal uEV nucleic acid (RNA) cargo (bar size = 10 μm). (D) Linear relationship between raw source sample dose (pre-clarified urine input) and isolated uEV particle concentration (output response) in samples processed by DC (left panel), SiC (middle panel) or PEG (right panel) methods.

non-vesicular contamination (Figure 3A). Isolated uEVs were either round or displayed a typical donut shape (EV drying artefact) and appeared structurally intact. Some uEV clusters were seen around the uromodulin fibres that appeared as long bright streaks. Tamm-Horsfall protein (THP), else known as uromodulin, is the most abundant urinary glycoprotein, and its presence was expected. According to TEM image analysis, the majority of uEXOs isolated by DC measured 50–120 nm in size, while the uMV fraction yielded larger vesicles ranging widely from 75 to 350 nm and that were scarcer (Figure 3A, left panel). This overlap in size aligns with the anticipated outcomes and shortcomings of the DC method (Livshits et al. 2015; Musante

et al. 2017). The SiC eluate, obtained through gravity flow during filtering out particles larger than 1.0 μm size, was concentrated by UC to match the final PA volume of other methods (Figure 3A, middle panel). While this optional particle concentration step, prone to introducing additional variations in uEV recovery (Benedikter et al. 2017), was omitted from our test-retest analysis, it could be considered in future investigations requiring a more concentrated final material. Since the abundance of uEVs isolated by PEG following a 6 h incubation at 1:10 (vol/vol) PEG to urine ratio was lower than that achieved by both DC and SiC, we opted for a 1:5 (vol/vol) ratio and an extended 24 h reaction time. In line with other reports, further increases in PEG concentration proved non-beneficial for both larger EV count and smaller particle size (Tangwattanachuleeporn et al. 2022). Some tiny 5–10 nm particles that were seen in PEG-derived samples, and confirmed by DLS technique, were consistent with PEG particle size (Figure 3A, right panel).

Conventional fluorescence microscopy of undiluted SYTO RNASelect dye-labelled PAs revealed detectable size vesicles that had an apparent nucleic acid (RNA) cargo (Figure 3B), whereas the images of PBS mixed with the same amount of dye alone and incubated under the same temperature and time conditions did not reveal any green-fluorescent light emitting structures. Furthermore, lysed PAs showed the presence of endogenous EV surface or internal protein markers such as tetraspanins (CD9), programmed cell death 6-interacting protein (ALIX), tumor susceptibility gene 101 protein (TSG101), glyceraldehyde 3-phosphate dehydrogenase (GAPDH) and Flotillin-1 (FLOT1) (Figure 3C). These proteins rank as #2, #3, #4, #6 and #7 among the TOP 100 EV-associated biomarkers in Vesiclepedia database and were observed in human uEV fractions by other investigators (Fernandez-Llama et al. 2010; Musante et al. 2012; Correll et al. 2022; Musante et al. 2013). The uEV samples were free of 140 kDa Cis-Golgi matrix protein GM130, 57 kDa endoplasmic reticulum lumen marker protein disulfide isomerase (PDI) or mitochondrial matrix-bound pyruvate dehydrogenase (PD) (Figure 3C). In addition, we could not detect mitochondrial outer or inner membrane proteins such as voltage-dependent anion channel (VDAC) or cytochrome c oxidase (COX IV) (data not shown). Except for naturally occurring isoforms, we did not detect any fragmented or degraded protein bands, proving a fair stability of uEVs in naïve biofluid over our procedural time limit.

3.2 | Short-Term Precision of Distinct uEV Isolation Methods

DC, SiC and PEG separate EVs from biofluids based on their molecular weight differences, pH-dependent affinity or co-precipitation reactions. To estimate and compare the short-term intra-laboratory precision (repeatability) of these three distinct EV isolation methods based on their ability to produce a *consistent* amount of particles displaying relatively uniform physiochemical characteristics, the concentration, mean size and modal size of uEVs was measured in multiple technical replicates (TRs). The TRs were generated by subdividing a single unique biological sample into k number of equal portions (Figure 1B). The size of urine collection containers typically ranges from 20 to 120 mL. The 50 ± 5 mL starting sample volume used for urine pre-clarification represented a typical clinical specimen collected for most diagnostic and pre-clinical studies. An optimal final volume of pre-clarified urine required for single TR was determined through a linearity analysis of input-output response curves (Figure 3D). Specifically, uMV and uEXO subpopulations that were isolated by the DC method utilised either 34 ± 0.5 or 33 ± 0.5 mL of urine, while isolations based on the uEV reactions with solid SiC or PEG matrixes, prone to extract smaller particles, used 30 ± 5 mL of urine per TR.

Table 1 and Figure S1 demonstrate a closeness of agreement among uEV concentration, mean and modal size values of multiple TRs generated from urine of different individuals using DC, SiC or PEG-based uEV isolation methods. Individual repeatability estimates were acquired through a single NTA data capture and analysis cycle: specifically, one final analyte (FA) that was prepared from each undiluted stock PA sample of TR_1 to TR_k underwent an examination over a single NTA run, comprising several repeated intra-sample measurements (RMs). The duration of these RMs was adjusted based on the observed particle density within an FA. They typically lasted either 0.5 or 1 min, deemed sufficient to generate a minimum of 1000 valid particle tracks. The qualifying values from all co-dependent longitudinal data points were averaged to calculate one FRV. The extent of between-TR (FRV-to-FRV) precision in each independent experiment was then expressed as a CV_{TR} percentage. The distribution of resultant individual CV_{TR} values within and among the distinct uEV isolation methods, as reported in Table 1, is also presented in Figure S2 for improved visual comparison.

To reduce the risk of measurement order-dependent artefacts in this set of experiments, the repeatability of each method was assessed using FAs adjusted to contain an optimal mid-range nanoparticle concentration per field of view (FOV), that is, frame, as recommended by NTA instrument's manufacturer. The appropriate concentration was determined in a separate test run: specifically, TR_1 to TR_k samples were combined into one master TR pool sample, which was then serially diluted to identify an FA containing approximately 45–75 PPF at a non-saturating camera sensitivity level. This number was estimated through NTA video data analysis using particle track detection threshold set to either 3 or 5, following their capture under relatively low sample flow speed equivalent to 8.4 ± 1 μL/min. The main advantage of non-stationary sample analysis is that due to continuous flow, unique particles are less likely to be counted more than once throughout all FOVs. Conversely, while improving repeatability, high sample flow speed negatively impacts nanoparticle counting and sizing accuracy.

Because statistically one repeatability assessment experiment would not carry too much weight, we conducted *recurring* test-retest experiments. Not every participant was able to deliver the specimen in a volume sufficient to generate 6 (~300 mL), let alone 12 (~600 mL) sub-samples. Thus, we were limited to employing only one selected uEV isolation method per biological sample per day, which was counted as one independent experiment. According to the sample size calculation formula provided by McAlinden et al. (2015), even though our population cohort for test-retest analysis was limited to a minimum of 8 and a maximum of 14 cases, it provided at least 85% confidence in estimating an average precision for each method of interest.

TABLE 1 | Technical performance of differential velocity centrifugation (DC), silicon carbide size-exclusion (SiC) or polyethylene glycol co-precipitation (PEG) methods based on isolated urinary extracellular vesicle (uEV) counting and sizing precision estimated by nanoparticle tracking analysis (NTA). Crude uEVs or specific uEV subpopulations (uMV or uEXO) were simultaneously isolated from multiple technical replicates (TRs) of single biological sample derived from different individuals across several independent experiments (n = 8–14). Particle concentration, mean size and modal size in each TR sample (TR#, k = 6 for DC, k = 8–12 for SiC or PEG) were measured under identical instrumental settings over a single analytical run. This run captured seven 30 s (uEVs and uEXO) or 60 s (uMV) videos of particles flowing at a steady speed (SPS = 35). The last recording was used to replace any one outlying repeated measurement (RM) value (if detected by the Grubbs test), the RM with a minimum value or otherwise was discarded before averaging six RM values to obtain one final reading value (FRV). The standard deviation (SD) of FRVs was multiplied by 100 and then divided by their arithmetic mean to calculate the individual coefficient of variation percentage for each group of TRs (CV_{TR}%). In the end, the pooled SD was divided by the grand mean of all FRVs to estimate average CV_{TR}% for each type of measurand, analyte and method.

Method	**DC**			**SiC**		**PEG**		**DC**		**SiC**	**PEG**	**DC**		**SiC**	**PEG**
Measurand	**Concentration**							**Mean size**				**Modal size**			
Analyte	uMV	uEXO	TR#	uEV	TR#	uEV	TR#	uMV	uEXO	uEV	uEV	uMV	uEXO	uEV	uEV
Individual CV_{TR} (%)	4.48	5.81	6	20.2	12	9.3	12	1.27	1.85	4.58	1.48	5.93	3.88	5.12	5.24
	4.12	5.89		12.9	10	14.2		0.94	1.19	2.21	2.91	6.59	1.71	4.16	5.59
	2.43	7.38		10.5	12	6.9		1.68	1.71	2.03	3.50	6.27	4.07	4.42	5.72
	5.15	6.30		17.4	12	13.2		2.28	0.92	3.08	4.07	2.51	5.10	6.61	5.22
	3.58	10.2		15.0	11	15.7		2.47	3.69	2.74	2.96	4.93	5.22	5.97	7.86
	4.41	5.03		14.8	10	9.5		1.25	0.91	2.27	3.15	2.72	3.86	9.46	6.81
	3.63	3.72		9.67	12	7.6		1.42	2.89	3.27	4.81	2.11	6.08	14.1	4.05
	4.85	6.57		11.4	8	19.3		2.42	4.11	3.01	2.22	6.25	4.23	7.29	4.20
	6.03	5.90		10.2	9			1.01	0.39	1.55		6.81	8.89	1.99	
	13.0	6.45						2.52	0.91			9.93	6.09		
	8.89	6.52						1.04	2.64			4.16	3.98		
	5.02	8.61						3.04	1.28			4.37	3.88		
	4.13	6.09						0.70	2.69			3.21	4.60		
	2.33	4.27						1.03	1.46			6.03	9.05		
	4.64	8.52						0.51	1.95			7.04	6.40		
	4.83	9.12						0.65	1.82			3.96	6.00		
Average CV_{TR} (%)	4.96	6.50		14.90		13.27		1.69	2.12	2.87	3.26	5.59	5.60	6.89	5.74
	5.73							1.90				5.60			

As seen from Table 1, the lowest average CV_{TR}% result highlighted that DC method clearly outperformed both SiC and PEG uEV isolation methods. DC was found to be the most repeatable in generating the NTA responses for all types of measurands. On average, the isolated uMV sub-population count (CV_{TR} = 5.0% vs. 6.5%) and mean size (CV_{TR} = 1.7% vs. 2.1%) data demonstrated slightly lesser dispersion than smaller uEXO particles, but this difference was insignificant ($p > 0.05$). Irrespective of isolated particle type, the degree of DC-associated repeatability for particle counting process (CV_{TR} = ~5.7%) was approximately 2.6-fold lesser than that of SiC (CV_{TR} = 14.9%) and 2.3-fold lesser than that of PEG (CV_{TR} = 13.3%) methods ($p < 0.0001$) (Figure S1, left panels). Similarly, the consistency of uEV sizing following their isolation by DC (average CV_{TR} of uMV and uEXO = 1.9%) was approximately 1.5-fold higher than that of SiC (CV_{TR} = 2.9%) and 1.7-fold higher than that of PEG (CV_{TR} = 3.3%) methods ($p < 0.0001$) (Figure S1, middle panels). This translated into a striking 88.9% or 79.4% difference for uEV concentration measurement repeatability estimates between the SiC or PEG and DC methods. For uEV mean size repeatability values, this difference was smaller (40.7% and 52.7%). The modal size measurements were also the most consistent across uEV samples derived by the DC method (CV_{TR} = 5.6%), with the PEG (CV_{TR} = 5.7%) and SiC (CV_{TR} = 6.9%) methods following behind (Figure S1, right panels).

TR samples generated by the SiC and PEG methods and gravity filtration were expected to be more uniform than those obtained by the DC, which did not include sample spin filtration (SF) step. However, when the imprecision of DC-derived uMV fraction particle measurements was compared before and after the SF, it tended to increase (Figure S3). One of the most plausible explanations for declined repeatability phenomenon after the SF step, is that the resultant samples had lost ~15% of larger sized-particles and therefore our pairwise before-after comparisons using a fixed dilution factor were in fact performed on different concentration range of analytes, which is known to impact the repeatability regardless of the method used to isolate uEVs, as shown in Figures S4 and S5.

Based on superior technical performance of DC over SiC and PEG methods regarding the consistency of isolated uEV counts and mean size, DC was further selected to be used in combination with other downstream uEV characterization techniques.

3.3 | Expanded Analytical Precision of Combined DC and NTA Methods

By using multiple TRs, we presented evidence that source sample processing has the potential to introduce differences in the composition of uEVs extracts, ultimately affecting the final test results of basic uEV characteristics. But so far, the precision was assessed relying only on a single FA preparation and a single FA measurement attempt, which by default excluded other potentially influential sources of variance. For instance, sub-sampling variations (CV_{FA}) focus on the discrepancies related to how viscous and heterogenous PA stock material is mixed and drawn from its container. It also encompasses differences in pipetting volumes, arising from inconsistent pipetting techniques while transferring aliquots from one tube to another. Instrumental measurement variations (CV_{RR}) are associated with the inherent characteristics and performance of the analytical device itself. They include aspects related to instrument calibration status between runs on different days, sensitivity influenced by wear and tear, the efficacy of instrumental part cleaning between runs performed on the same day, and device stability due to external conditions (see Figure 1). Suchvariations also reflect differences in the response of the instrument to different types and concentration ranges of the measurand/analyte.

To obtain more representative short-term analytical precision CV_A estimates for the best performing method (DC) in conjunction with NTA, we employed the following sample analysis workflow: three aliquots were drawn from each TR ($k = 6$) to prepare 3 FAs ($l = 3$). Each FA was then analyzed over three RRs ($m = 3$). Each run comprised of six longitudinal repeated intra-sample measurements (RMs) ($p = 6$). The percent contribution of corresponding TR, FA and RR variance components towards the total variance (TV) of uEV characterisation by NTA process was assessed by fully nested random-factor ANOVA and presented as VCA pie charts (Figure 4). Individual CV_{TR}, CV_{FA} or CV_{RR} values were presented inside each pie chart created for either uEXO (Figure 4A) or uMV (Figure 4B) particle concentration (Figure 4, left panels) or mean size (Figure 4, right panels) measurands. Their sum representing gross technical/analytical error CV_A was indicated outside the pie chart area. Based on formulae presented in Figure 1, the CV_A was calculated for two separate scenarios: (a) while taking into consideration within-RR (between-RM) measurement error ($CV_W = CV_{RM}$) (Figure 4, upper panels) or while ignoring it (Figure 4, bottom panels). While the latter is more appropriate, the former is informative as it raises analyst's awareness about the extent of co-dependent intra-sample variations due to highly heterogenous and polydisperse nature of our sample. Familiarity with the routine technical intra-sample noise in NTA may be helpful in spotting unusual patterns (e.g., drifts) in data and identifying potential outliers.

As seen from Figure 4 results, overall precision of concentration measurements was markedly better in uMV than in uEXO fraction particles (~5.5% vs. 9.6%). By contrast, the repeatability of sizing was nearly twice as good in smaller uEXO than in larger uMV particle samples (~1.1% vs. 2.0%). According to VCA of fitted ANOVA model that excluded within-run (CV_{RM}) errors, procedural variations had the most influence on both uEXO and uMV counting precision (Figure 4, bottom left panels), whereas instrumental measurement variations were more impactful in uEXO and uMV particle sizing (Figure 4, bottom right panels). The inclusion of RM variance component in the fitted ANOVA model, resulted in higher CV estimates for all types of uEVs and their measurands (Figure 4, upper panels).

If procedural and/or sample draw variations account for substantial imprecision during uEV assessment process, the logical question is whether TR and FA sample pooling is a suitable strategy to eliminate these errors? Repeatability of uEV concentration, size, or protein content measurements before and after elimination of such variations is analyzed in Figure 5. Figure 5B presents evidence that the size distribution and concentration measurement results of pooled TRs generated from one biological source sample by DC (as shown in Figure 5A) fairly matched their arithmetic mean. After evaluating these effects across multiple independent experiments, we concluded that the percentage dif-

TABLE 2 | Combined procedural and instrumental precision of differential velocity centrifugation (DC)–based isolated urinary microvesicle (uMV) fraction particle measurements by SLAM microscopy. uMVs were simultaneously isolated from multiple technical replicates (TRs) of single biological sample across independent experiments ($n = 17$). Particle 2PF, 3PF, THG intensity and derivative total uEV count as well as ORR signals were co-measured under identical instrumental settings over a single analytical run that evaluated a minimum of 25 field of view (FOV) locations within each TR. The standard deviation (SD) of averaged FOV values was multiplied by 100 and then divided by their arithmetic mean to calculate the individual coefficient of variation percentage for each group of TRs (CV_{TR}%). In the end, the pooled SD was divided by the grand mean of all TR values to estimate average CV_{TR}% for each type of measurand.

Measurand	2PF	3PF	THG	EV count	ORR	TR#
Individual CV_{TR} (%)	20.0	13.3	13.1	49.0	0.56	6
	11.9	6.9	14.0	29.1	0.54	6
	8.9	9.3	16.3	15.8	0.17	5
	6.5	4.4	19.6	21.1	0.22	6
	5.3	2.5	4.4	24.9	0.30	6
	13.9	7.0	14.7	56.2	0.41	6
	4.8	12.9	11.5	150.4	0.74	5
	5.7	2.0	10.3	9.7	0.35	6
	4.4	3.9	6.5	15.3	0.33	4
	12.6	10.1	10.6	8.8	1.46	6
	10.0	3.5	8.6	26.1	0.38	6
	3.0	4.4	9.7	27.3	0.04	6
	8.6	12.6	9.6	39.6	0.06	6
	58.1	38.5	48.8	104.8	0.30	6
	6.7	7.6	5.4	21.3	0.07	6
	7.0	1.7	3.7	14.6	0.14	6
	9.5	38.5	6.3	49.0	0.25	6
Average CV_{TR} (%)	28.5	13.8	22.0	30.2	0.5	

ferences between the pool and arithmetic mean of individual TRs did not exceed 5% or 10% for uEV mean size and concentration measurands in NTA, respectively. Similar effect was observed for alternative SiC and PEG-based uEV isolation methods coupled to NTA analysis (Figure S6).

As expected, in a scenario, where six isolated uEXO TR samples ($k = 6$) were first pooled into one master TR sample ($k = 1$) and then used to generate seven FAs ($l = 7$) that were in turn analyed by three successive RRs ($m = 3$) (Figure 5C), the combined $CV_A = (CV_{FA}^2+CV_{RR}^2)^{1/2}$ values for both concentration (4.23%) and size (0.94%) were lower than $CV_A = (CV_{TR}^2+CV_{FA}^2+CV_{RR}^2)^{1/2}$, which included procedural variations as seen from Figure 4A, bottom panel results (~9.6% and ~1.1%). Assessment of readout dependency on FA order revealed no systemic effects (Figure 5C, left panel). Finally, in a representative scenario, where both TR- and FA- variance components were eliminated by a strategy of six TR ($k = 6$ to $k = 1$) and subsequent seven FA ($l = 7$ to $l = 1$) sample pooling, the analytical precision CV_A, now reflecting only the extent of instrumental run-to-run errors CV_{RR}, was approximately 5.1%, 0.9% and 10.3% for uEXO particle concentration, mean size and modal size measurements, respectively (Figure 5D). The corresponding estimated CV_A for uMV fraction particles resulted in 4.2%, 1.4% and 12.4% values. These values were later used to verify if combined analytical DC-NTA method performance meets the desired, optimal or minimal analytical imprecision goals (see Table 3).

The elimination of procedural sample processing variations improved the repeatability of other uEV isolation methods used in this study. For example, in a scenario, where twelve PEG-derived uEV TR samples ($k = 12$) were pooled ($k = 1$) and then used to generate 12 FAs ($l = 12$) that were in turn analyzed over single run ($m = 1$) after spin-filtering, the resulting CV_A was on average 3.2% for concentration, and 0.9% for mean size measurements by NTA technique (Figure S7). This is a dramatic improvement when compared to the previously reported precision estimates (13.3% and 3.3%) reported in Table 1, although the repeatability of modal size measurements remained unchanged (5.75% vs. 5.74%). Repeatability estimates for uEV measurements by NTA after elimination of both procedural sample processing and sample draw variations in SiC- or PEG-based uEV isolation methods are presented in Figure S8. In this protocol, 12 TRs ($k = 12$) were pooled into one master TR sample ($k = 1$), which was subsequently used to draw, and then pool seven FAs ($l = 7$ to $l = 1$). Thirteen ($m = 13$) RRs were executed in NTA resulting in CV_A of 5.0% and 4.4% for SiC- or PEG-derived uEV particle counts, 0.9% and 3.4% for mean size or 5.6% and 7.9% for modal size measurands. In conclusion, TR and FA pooling is a suitable strategy to improve short-term precision of uEV mean size and

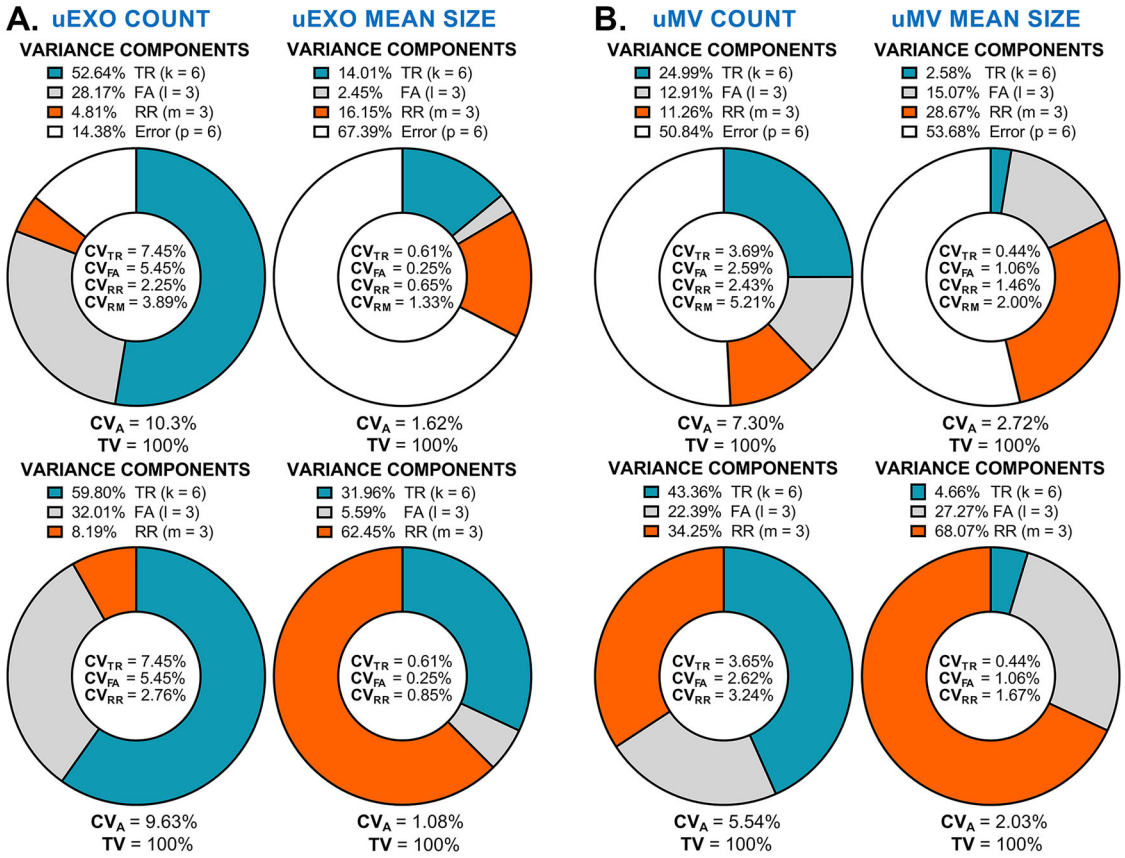

FIGURE 4 | Variance component analysis (VCA) of urinary extracellular vesicle (uEV) concentration and mean size measurements by nanoparticle tracking analysis (NTA) following uEV isolation by differential velocity centrifugation (DC) method. Six technical replicates (TRs, $k = 6$) of one biological sample ($N = 1$) were used to isolate urinary exosome (uEXO) (A) or microvesicle (uMV) (B) enriched fractions that were consecutively sampled to prepare three appropriately diluted final analytes (FA, $l = 3$). Particle concentration (*left panels*) and mean size (*right panels*) in each FA were measured over three replicated runs (RRs, $m = 3$) under identical instrumental data capture and analysis conditions. Expected mean square values were estimated by nested random factor ANOVA to find out how much of the total variance (TV%) in typical NTA results might be attributed to the sample processing (TR) and sample draw (FA) differences and how much to instrumental RR-associated error, which was calculated either considering (upper panels) or ignoring (bottom panels) random within-run fluctuations of six 60 s long repeated intra-FA measurements (RM). Derivative coefficient of variation percentage (CV%) values for individual variance components are shown inside pie charts. Combined analytical precision CV_A values are indicated at the bottom of each chart.

concentration, but not necessarily modal size measurements by NTA.

3.4 | Analytical Precision of Combined DC and IB Methods

Next, we performed the consistency analysis of structural and endogenous DC-derived uEV protein cargo. In our hands, the uEV-associated protein concentration measurement repeatability by Multi-strip Western Blotting (MSWB) technique, a higher throughput comparative immunoblotting (Figure 6A), varied depending on the uEV fraction type, origin and antigen of interest. For instance, the CV_{TR} of uEXO protein marker Alix expression was on average 9.3%, whereas uMV-associated Alix measurements were less sporadic ($CV_{TR} = 5.1\%$) ($N = 6$) rendering the average CV_{TR} = 6.5% (Figure 6B). Similarly, the CV_{TR} of TSG101 expression among the TR1-TR6 samples within uEXO and uMV fractions was on average 10.1% and 6.7%, respectively, with an average $CV_{TR} = 7.2\%$ ($N = 6$). The protein marker PKM1/2 was expressed more evenly and displayed an average $CV_{TR} = 5.9\%$ with CV_{TR} distribution of 4.4% and 5.9% in uEXO and uMV fractions, respectively (Figure 6B). The GAPDH levels in TR1-TR6 were fluctuating with $CV_{TR} = 6.6\%$ in male and $CV_{TR} = 11.2\%$ in female uMV samples, or CV_{TR} = 6.0% and CV_{TR} = 7.5% in male and female uEXO samples, respectively (Figure 6B). Interestingly, the procedural variations of other uEV proteins were also consistently lower in male ($N = 3$) compared to female ($N = 3$) uEV samples (e.g., CV_{TR} = 9.7% vs. 8.9% for Alix, CV_{TR} = 7.5% vs. 8.5% for TSG101, $CV_{TR} = 4.8\%$ vs. 3.4% for PKM1/2).

The second and ninth lanes in 4%–12% gradient gels (immediate before and after the molecular weight marker lanes) were loaded with pooled master TR7 sample. To minimise protein transfer variability, up to four gel strips containing an antigen of interest in the middle were arranged onto same nitrocellulose membrane, resulting in one individual blot (Figure S9). The analysis of four blots per uEXO or uMV fraction isolated from male or female volunteer urine by DC method was performed after protein band baseline detection using 'Morphological' method

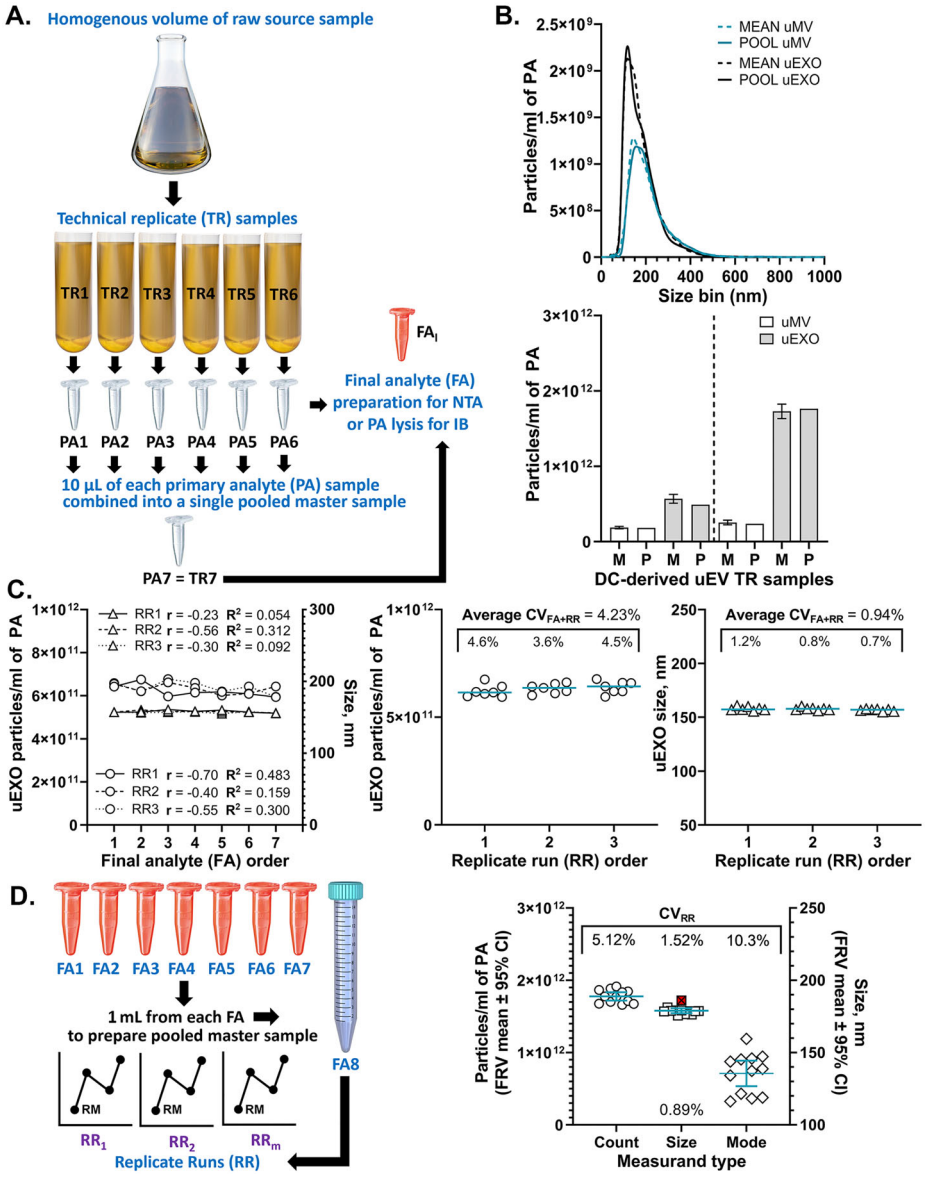

FIGURE 5 | Repeatability of urinary extracellular vesicle (uEV) concentration and size measurements by NTA before and after elimination of procedural sample processing and/or sample draw variations by sample pooling. (A) A diagram showing the principle of biological source sample division and subsequent pooling. (B) Concordance of pooled sample NTA measurement values with the mean of individual technical replicates (TR). Upper panel. NTA particle count and size distribution graph showing the arithmetic mean of six TRs (*dashed lines*) plotted against pooled TR master sample data (*solid lines*) for urinary microvesicle (uMV, *teal lines*) or exosome (uEXO, *black lines*) enriched fractions separated by differential velocity centrifugation (DC) method. Bottom panel. Bars represent the area under the curve, reflecting total detected particle number per 1 mL of primary analyte (PA). The mean of each individual TR analyte (M) is compared to the corresponding pool of six TRs (P) across two individuals (separated by *dashed vertical line*). (C) Repeatability of uEXO measurements by NTA after elimination of procedural sample processing variations. Six TRs ($k = 6$) were pooled into one master TR7 sample, further used to draw seven final analyte (FA) samples ($l = 7$). Particle concentration (*circle symbols, left Y axis*) and mean size (*triangle symbols, right Y axis*) in each FA were measured over three replicate runs (RRs; $m = 3$). Readout dependency on FA order is shown in the left panel with corresponding Pearson correlation coefficient (r) and R squared values. Readout dependency on RR order is shown in the middle and right panels. Horizontal line within each RR group represents the mean of 7 FA values for uEXO concentration (middle panel) or size (right panel) measurements. Combined sample draw and instrumental read precision was estimated by single random factor ANOVA and expressed as coefficient of variation percentage (%) CV_{FA+RR}. Differences among FAs accounted for 6.13% and 5.63% of total variance in uEXO counting and sizing procedures, respectively. (D) Repeatability of uEXO measurements by NTA after elimination of procedural and sample draw variations. Six TRs were pooled into one master TR7 sample as described above. Seven individual FAs were prepared from TR7 and then pooled into one master FA8 sample (left panel) later diluted to yield on average 68 ± 3 particles per frame. Particles within FA8 sample were analyzed over 12 RRs. Each RR consisted of six 30 s long RM videos captured at fixed CL = 14, SPS = 35, and analyed at DT = 3 NTA settings. RM values were averaged at the end of the run into single final reading value (FRV). Horizontal lines and error bars in the right panel represent the mean and 95% confidence interval of FRVs of uEXO concentration (*circle symbols, left Y axis*), mean size (*square symbols, right Y axis*) and modal size (*diamond symbols, right Y axis*). Relative uncertainty of uEV measurements was expressed as CV_{RR} to assess instrumental intra-day between-run precision. Any outlying values detected by Grubbs test at 95% confidence level are indicated by red crossed symbols, and CV_{RR} shown below the scatter plots is computed after outlier elimination.

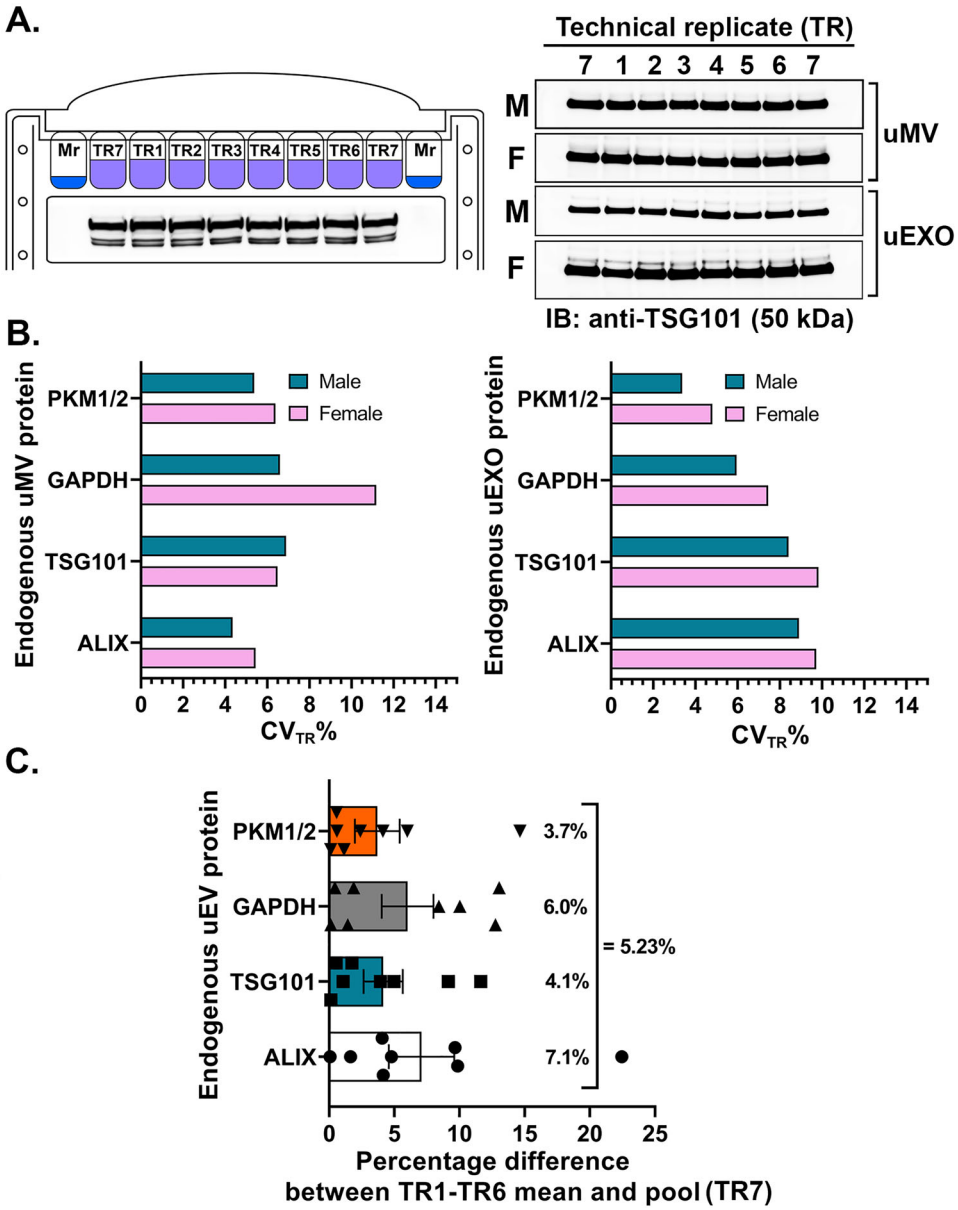

FIGURE 6 | Repeatability of selected urinary extracellular vesicle (uEV) protein content measurements by Multi-Strip Western Blotting (MSWB). (A) The principle of MSWB analysis. Multiple gels were loaded with molecular weight marker (Mr, lanes 1 and 10) and lysates of either individual technical replicate (TR) samples (lanes 3–8) or pooled master TR7 sample in duplicate (lanes 2 and 9) prepared by mixing equal amounts of TR1–TR6 lysates of either uMV or uEXO fractions to resolve proteins by their molecular weight (left panel). After electrophoresis, these gels were cut into strips. Strips that contained the identical antigen of interest, were aligned onto single assembling filter paper, and then transferred onto single nitrocellulose membrane. Following protein transfer, the membrane was blocked and probed with appropriate primary and HRP-conjugated secondary antibodies. For visualization, some strips were rearranged to alternate between male (*M*) and female (*F*) subjects and between uEXO and uMV series, because paired samples were loaded in a randomised manner. Black line strokes around the individual strips were drawn to improve readability. The representative blot shows 50 kDa TSG101 protein level distribution across TR1-TR7 samples of paired uEV fractions of individual subjects (right panel). (B) Comparison of procedural sample processing precision for selected endogenous uEV protein detection following uEV isolation by DC method. Relative uncertainty of chemiluminescent protein band signal measurements was expressed as CV_{TR} to assess average procedural sample processing precision in six uMV (*left panel*) or six uEXO (*right panel*) TR samples obtained from male (*teal bars*) ($N = 3$) or female (*pink bars*) urine ($N = 3$) by differential velocity centrifugation (DC) method. (C) Comparative uEV-associated protein marker expression levels before and after elimination of procedural sample processing variations by sample pooling. Average percentage difference calculated between the arithmetic mean of signal detected across six individual TR samples for PKM1/2 (*upside triangle symbols*), GAPDH (*triangle symbols*), TSG101 (*square symbols*) and ALIX (*circle symbols*) protein bands and an average signal of pooled (TR7) sample, which was loaded in duplicate. The analysis was performed on 8 data points (4 uMV and 4 uEXO series).

TABLE 3 | Calculation of index of individuality (IOI) and reference change values (RCV) at $p < 0.05$ based on the biological and technical/analytical variability of DC-derived urinary exosome (uEXO) or microvesicle (uMV) fraction particle concentration, mean size and optical redox ratio (ORR). Except for ORR, combined analytical coefficient of variation (CVA, in %) was estimated after exclusion of procedural and sample draw errors, as described in the text.

Measurand	uEV type	CV_G (%)	CV_I (%)	Goals for analytical imprecision (%)			Estimated CV_A (%)	IOI	Unidirectional RCV (%)	Bidirectional RCV (%)
				$0.25 \times CV_I$	$0.5 \times CV_I$	$0.75 \times CV_I$				
Concentration	uMV	63.0	32.2	8.1	16.1	24.2	4.2	0.52	75.3	90.0
	uEXO	54.0	23.2	5.8	11.6	17.4	5.1	0.44	55.1	65.8
Mean size	uMV	6.91	5.62	1.4	2.8	4.2	1.4	0.84	13.4	16.1
	uEXO	8.51	4.78	1.2	2.4	3.6	0.9	0.57	11.3	13.5
ORR	uMV	1.08	1.49	0.4	0.7	1.1	0.7	1.52	3.8	4.6

with 10% peak width tolerance. The mean of protein band signal intensity derived from lanes 3 to 8 containing TR1 to TR6 samples, respectively, were compared to the average signal of two TR7 sample protein bands. There was a mean 5.23% difference between the endogenous uEV biomarker signal intensity level in the TR pool and the mean signal of six individual TRs assessed by MSWB in DC-derived uEV protein lysates ($N = 8$ data points) (Figure 6C). This value fell inside the 5%–10% range of pooled versus individual sample concentration differences earlier observed by NTA.

3.5 | Analytical Precision of Combined DC and DLS Methods

A similar experimental design of 6 TRs, 3 FAs and 3 RRs was created to assess the short-term precision of hydrodynamic diameter (HD) and polydispersity index (PDI) evaluation in DC-derived uEV samples by the DLS technique (Figure 7). As seen from the bar graphs (Figure 7A,B) and VCA pie charts (Figure 7C) created for uMV and uEXO fraction particles, instrumental run-to-run variations contributed the most to the total variability (TV) of HD measurements. However, these variations decreased once we employed a manual focus adjustment method to capture sequential RR data and increased the RR number. TR pooling closely matched the arithmetic mean of both uMV and uEXO TR samples, and generated number-, intensity- and volume-weighted size distribution curves with largely comparable area under curve values (Figure 8A). Effective pooling was also seen for TRs derived by less precise SiC or PEG-based uEV isolation methods (Figure S6). After eliminating the procedural sample processing errors, the CV_A of uEXO HD measurements decreased from 8.15% to approximately 2.93% (Figure 8B, upper panel), whereas PDI was below 10% (Figure 8B , bottom panel). Once sample draw errors were reduced by further FA pooling, the resulting CV_A of HD measurements reached ~2.8% for uEXO and 1.7% for uMV particles (Figure 8C, upper panel), whereas PDI was below 10% (Figure 8C, bottom panel). In general, the PDI of uMV was larger than that of uEXO samples, suggesting greater heterogeneity, but it did not exceed 30%, indicating that analyzed samples were largely free of aggregates. The repeatability of PDI measurements in DC-derived uMV and uEXO samples as assessed by 12 RRs, was 3.9% and 5.0%, respectively (Figure 8C, bottom panel).

3.6 | Analytical Precision of Combined DC and SLAM Microscopy Methods

Metabolic indicators can fluctuate with time, even over short periods, based on cellular activity, environmental conditions or metabolic cycles. Variations in timing could lead to different metabolic states at the time of measurement. Therefore, next we evaluated the precision of functional metabolic activity indicator ORR measurements in DC-derived uMV fraction samples by SLAM microscopy.

Due to the expected biological intrinsic uMV particle heterogeneity, 2PF and 3PF signals were evaluated in at least 25 random FOV locations within each TR sample. These FOVs contained a different amount of scattered semi-immobilised particles assessed

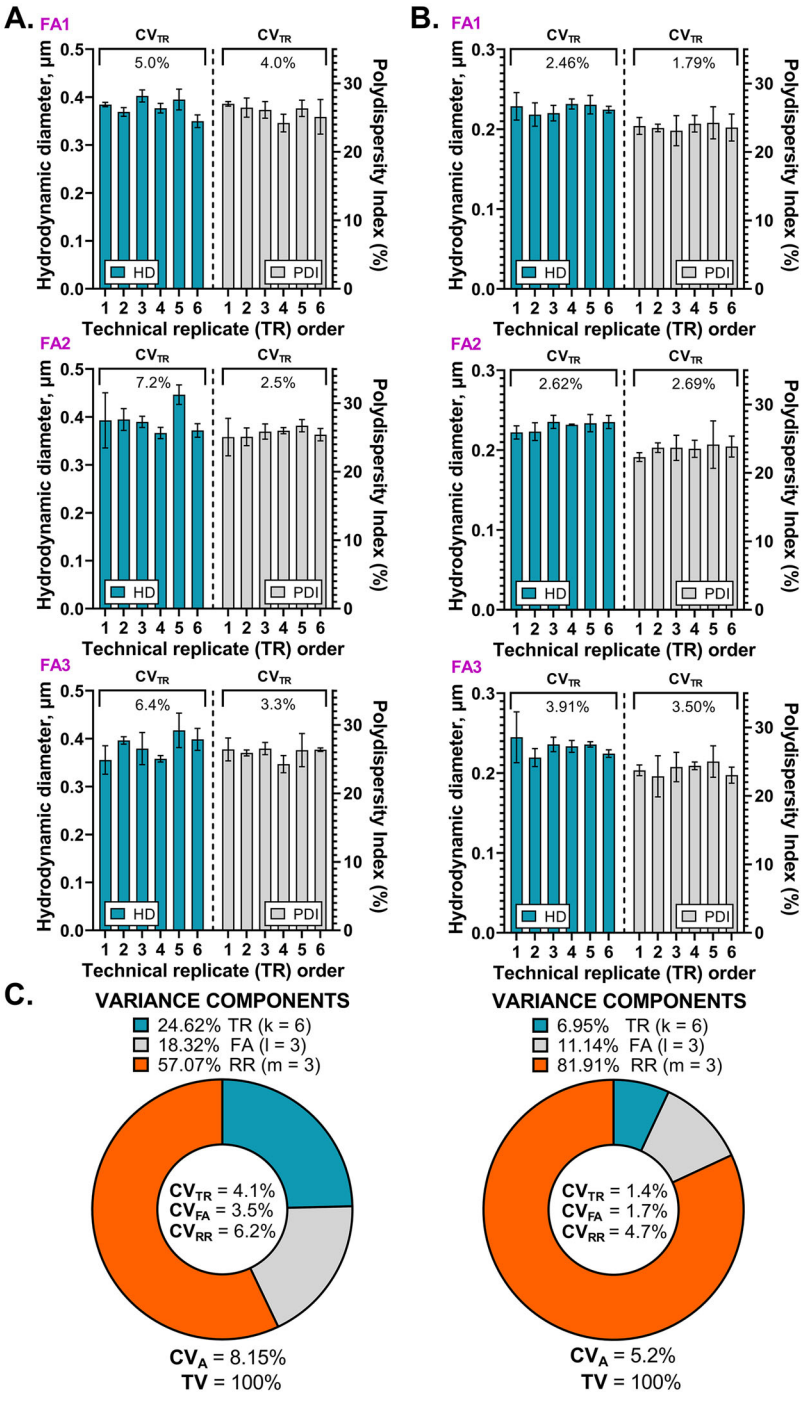

FIGURE 7 | Variance component analysis (VCA) of urinary extracellular vesicle (uEV) hydrodynamic diameter (HD) and polydispersity index (PDI) measurements by dynamic light scattering (DLS). uMV (A) or uEXO (B) particles were isolated from six technical replicates (TRs, $k = 6$) of single biological source sample by differential velocity centrifugation (DC) method. Each TR was used to prepare three final analyte (FA, $l = 3$) samples that were measured over three replicate runs (RRs, $m = 3$) under identical instrumental data capture and analysis conditions. Each RR consisted of ten 30 s long repeated measurements (RMs) that were averaged at the end of the run into single final reading value (FRV). Bars with errors indicate the FRV±SD of three RRs for the HD (left plots, *teal bars*) or PDI % (right plots, *grey bars*) measurands in FA1 (*upper panel*), FA2 (*middle panel*) or FA3 *(bottom panel*) sample draw conditions. Pie charts (C) display the estimates of the contribution of different random sources of variation (TR, FA or RR) to the total variance (TV%) of uMV (left panel) and uEXO (right panel) particle HD measurements by DLS. Derivative coefficient of variation percentage (CV%) values for individual variance components are shown inside pie charts. Combined peri-analytical precision estimate (CV_A) is indicated at the bottom of each chart.

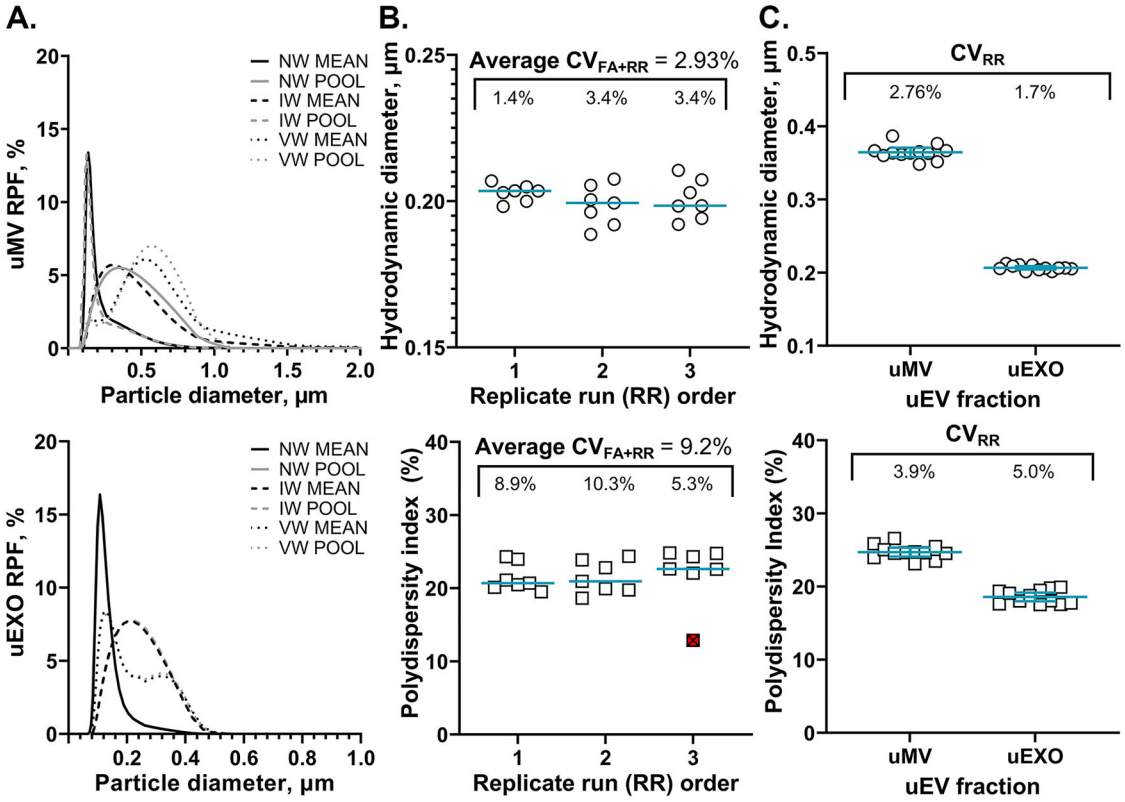

FIGURE 8 | Repeatability of urinary extracellular vesicle (uEV) size measurements by dynamic light scattering (DLS) after removal of procedural sample processing and sample draw variations by sample pooling. (A) Concordance of pooled sample DLS measurement values with the mean of individual technical replicates (TR) for uMV (upper panel) and uEXO (bottom panel) size distribution results. The arithmetic mean of six TRs (*black lines*) for number-weighted (NW, *solid lines*), intensity-weighted (IW, *dashed lines*) or volume-weighted (VW, *dotted lines*) relative particle frequency (RPF) data was plotted against pooled TR master sample values (*grey lines*). (B) Repeatability of uEXO measurements by DLS after removal of procedural sample processing variations. Six TRs ($k = 6$) were pooled into one master TR7 sample, further used to draw seven final analyte (FA) samples ($l = 7$). The hydrodynamic diameter (HD) (upper panel) and polydispersity index (PDI) (bottom panel) in each FA were measured over three replicated runs (RRs, $m = 3$). Horizontal lines within RR groups represent the means of FAs. Precision was estimated by a single random factor ANOVA and expressed as CV_{FA+RR} after removal of any outlying values detected by Grubbs test at 95% confidence level (indicated by red crossed symbols). (C) Repeatability of uEV measurements by DLS after removal of both procedural sample processing and sample draw variations. Six TRs of DC-derived uMV or uEXO fractions were pooled into one master TR7 sample, subsequently used to draw, and then pool seven FAs. Particle HD (upper panel) or PDI (bottom panel) were analyzed over 12 RRs. Each RR consisted of ten 30 s RMs that were averaged at the end of the run into single final reading value (FRV). Horizontal lines and error bars represent the mean and 95% confidence interval of FRVs. Relative uncertainty of uEV measurements was expressed as CV_{RR} to assess instrumental intra-day between-run precision. Any outlying values detected by Grubbs test at 95% confidence level are indicated by red crossed symbols, and CV_{RR} shown below the scatter plots is computed after outlier elimination.

by the THG channel, where signals are elicited by water-lipid and water-protein interfaces (Weigelin et al. 2016). Each FOV was imaged once over a brief period (8 s) and the mean signals were calculated as described under Section 2. Individual and average CV_{TR} values calculated for the 2PF, 3PF, THG intensity, uEV count as a function of THG, and derivative ORR measurands across 17 independent experiments are presented in Table 2. Average CV_{TR} of ORR measurements was 0.5%.

To evaluate the contribution of additional sample draw errors, each of six TRs generated from one biological sample ($k = 6$) was used to make five FAs ($l = 5$). The patterns of average ORR readouts collected across 25 FOVs, 5 FAs or 6 TRs can be seen from Figure 9, which presents two distinct cases of morning urine analysis from two males of comparable age at three different days. In the first case presented in Figure 9A, the uMV isolation procedure by DC on Day 1 (Figure 9A, upper panel) resulted in one significant outlier (TR6), which had to be removed from the rest of data before calculating the CV_{TR}. Sample draw imprecision was higher than procedural sample processing imprecision (CV_{FA} = 0.7% vs. CV_{TR} = 0.6%) but was in general exceedingly small. Lower ORR measurement precision due to procedural sample processing errors was observed on Day 2, whereas variations caused by sample draw order were smaller (Figure 9A, middle panel). There were no obvious issues with ORR measurement repeatability on Day 3 (Figure 9A, bottom panel). The mean CV_A of Day 1–3 was 0.82%. In the second case (Figure 9B), Day 1 yielded the most scattered ORR values across FOVs (Figure 9B, upper panel), and slightly larger CV_{FA} compared to CV_{TR} (0.3% vs. 0.1%). Interesting systemic sample draw order-dependent patterns were seen on Day 2: ORR tended to increase with each subsequent FA starting from TR #2 to TR #6 (Figure 9B, middle panel), although in general CV_{TR} was larger than CV_{FA} (0.5% vs. 0.3%). Finally, ORR measurements on Day 3 revealed that the very first

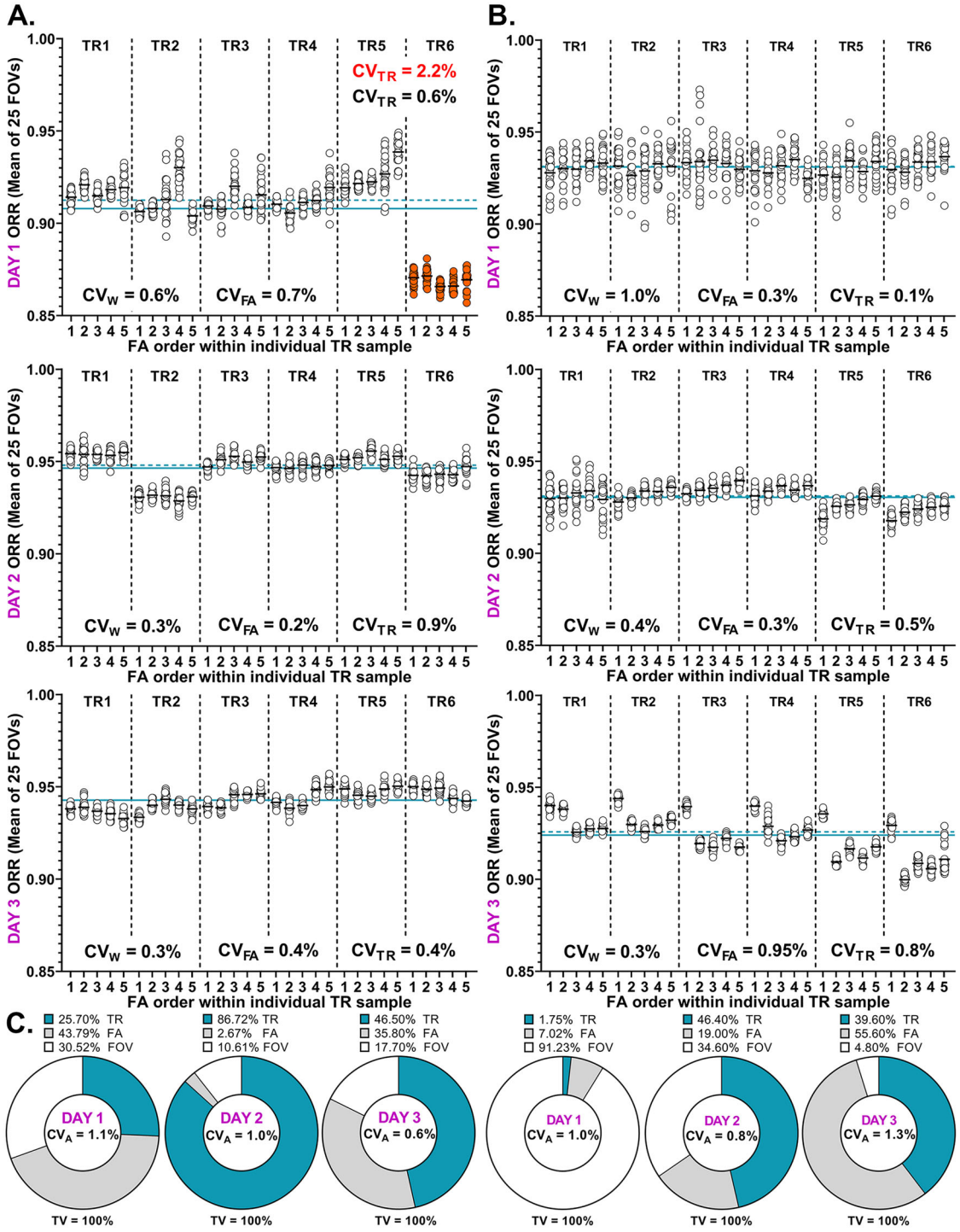

FIGURE 9 | Combined peri-analytical precision of biophysical urinary extracellular vesicle (uEV) characterisation by SLAM microscopy. Morning urine was obtained from individuals #1 (A) or #2 (B) on three different occasions (Days 1, 2 and 3). Six technical replicates (TRs, $k = 6$) created per biological source (raw) sample were subjected to differential velocity centrifugation (DC) to isolate urinary microvesicle (uMV) fraction. Resulting primary analyte (PA) was consecutively sampled to prepare five appropriately diluted final analyte (FA) samples ($l = 5$). Optical redox ratio (ORR) of particles in each FA was measured under identical instrumental data capture and analysis conditions over a minimum of 25 random field of view (FOV) locations. This measurement was considered a single run. The mean of 25 ORR values (*white circle symbols*) per FA are shown as black shot horizontal lines. The grand mean or grand median of all mean ORR values is shown as teal horizontal solid or dashed lines, respectively. Outlying FA and/or TR values are shown as colored symbols. Derivative CV% values for individual variance components are shown inside the temporal plots. Red values indicate CV_A prior to removal of any FA or TR outliers. For variance component analysis (VCA), displayed as pie charts (C), the expected mean square values were estimated by nested random factor ANOVA to find out how much of the total variance (TV%) in typical SLAM results might be attributed to the procedural sample processing (TR-to-TR) and sample draw (FA-to-FA) differences and how much to random instrumental within-run error. Combined CV_A values for different days are indicated inside pie charts.

sample draw provided the largest ORR estimate, while other FA-associated ORR values were smaller (Figure 9B, bottom panel). The mean CV_A of Day 1–3 was 0.71%. The results of associated VCA that considered random FOV-to-FOV measurement variations (CV_W) are shown in Figure 9C. In this case, CV_W represents an inherent degree of ORR heterogeneity within a biological sample. Even though the expected combined CV_A for ORR evaluation by SLAM microscopy was on average 0.77%, in ideal cases the variations were minimal, resulting in exemplary $CV_A = 0.1\%$ (Figure S10).

The experimental design presented in Figure 9 did not include instrumental variations arising from multiple RRs of the same FOV, because caution required with nonlinear multi-photon microscopy relates to the laser power directed towards a biological specimen. With higher power or longer exposure time, tissue, cell and potentially EV damage may quickly occur and might be mistaken for the biological effect (Sanderson et al. 2014). Moreover, despite a partial immobilisation within the viscous glycerol bed, the EVs within one FOV could diffuse and shift with time. Despite these challenges, we sought to assess any time-dependent cumulative thermal or other effects SLAM power might have had on the uMV particles. In a separate experiment, the same FOV of six TR samples ($k = 6$) or their pool (TR7) was serially imaged up to fourteen times ($m = 14$). The cumulative time-courses for the 2PF, 3PF, THG (uEV count within FOV) and ORR signals were constructed along with the linear trendlines, associated goodness of fit (R-squared) as well as Pearson correlation coefficient (r) values (Figure S11A). Due to particle diffusion, there was on average a 15% drop in particle counts within the same FOV over approximately 2-min total sample imaging time (Figure S11A, upper left panel). Within this brief period, mean ORR values tended to increase ($r = 0.73$, $p = 0.003$), with approximately 0.5% percent change between the first and last value and 0.70% percentage difference between the minimal and maximal observed values (Figure S11A, bottom left panel). These changes were mostly attributed to the FAD autofluorescence signal emitted from the 2PF channel that appeared to be the most sensitive to cumulative SLAM laser exposure ($r = 0.62$, $p = 0.019$) (Figure S11A, upper right panel). TR sample pool with $CV_{RR} = 0.63\%$ showed a comparable ORR response to that of arithmetic TR mean (Figure S11A, bottom middle and right panels). According to one-way random factor ANOVA, the contribution of procedural sample processing variations to the total variance (TV%) of uMV ORR measurement process increased with a decreasing number of RRs, resulting in a cumulative CV_A varying between 0.72% and 0.83% (Figure S11B).

3.7 | Biological Variability of uEVs

Biological intra-individual variations may be short- (within-day), intermediate- (between-day) and long-term (monthly, bimonthly, semiannual). Upon the examination of diurnal uEV changes in a limited cohort of healthy male and female individuals, it was found that the first morning urine void consistently contained higher uEV concentration than the urine collected either in the afternoon or in the evening of the same day. There was at least a 6-h gap between these three biological sample collection events from the same individual. These variations were observed in both genders for both types of uEVs (Figure 10A, upper panel). Thomas et al. demonstrated significant urinary protein concentration differences between the first morning, the second morning and random, single-void spot urine collection events (Thomas et al. 2010), and it is likely uneven uEV concentration (and thus their cargo) contributed to these differences. However, there were no significant differences in mean particle size (Figure 10A, bottom panel) or ORR values (Figure 10B) between the AM and PM samples, although according to DLS analysis, the uMVs collected in the AM tended to be smaller than those collected in PM (Figure S12).

The size distribution patterns of uMV and uEXO particles that were isolated from a morning urine of the same individual did not dramatically differ over an intermediate (2 week) period (Figures 10C and S13). By contrast, the long-term bimonthly intra-individual variations could reach over 30% for uEV concentration (Figure 10D, upper panel) and 8% for mean size (Figure 10D, bottom panel). The distribution of average intra-individual variation CV_I estimates calculated from at least three time points per individual for different DC-derived uEV fraction measurands (EV concentration, size and ORR) are presented in Figure 10E. These CV_I estimates were used to calculate the goals for analytical imprecision (Table 3). For all measurands, except the ORR, the magnitude of analytical precision CV_A met the desired method performance index ($CV_A \leq 0.25 \times CV_I$). The analytical precision of uMV ORR measurements was optimal ($CV_A \leq 0.5 \times CV_I$).

Lastly, the biological uEV concentration, size and ORR variability (CV_G) was assessed among all healthy subjects that participated in this study (Figure 10F). Together with CV_I and observed CV_A estimates, CV_G was used to quantify the IOI and RCV percentage values (Table 3). The IOI between 1.4 and 0.6 was attributed to the uEV size measurements, suggesting that both population- and individual-based RI could be used while exercising caution. The IOI < 0.6 results for DC-derived uEXO and uMV concentration suggested that individual-based RI may be more suitable for interpretation of changes in diagnostic/prognostic laboratory test results of these measurands. By contrast, the IOI > 1.4 suggested that population-based RI may be more suitable for interpretation of ORR changes. Since the ORR mean of healthy subjects was 0.974 and the one-sided RCV was 3.8%, if the mean ORR of unknown subject would be lower than 0.937, it would be considered outside the desired range, and unlikely to be due to the combined effects of analytical and biological variation.

4 | Discussion

There is a continuously growing list of uEV-associated proteins and miRNAs with potential diagnostic and prognostic value reported in the literature (Tepus et al. 2022). Nonetheless, the physical characteristics and functional properties of uEVs may also serve as the primary or complementary secondary biomarkers of health and disease. A priori knowledge of analytical precision (CV_A) associated with specific uEV separation and characterisation methods, as well as the measurand of interest within the useful selected analyte detection range, is particularly needed when biological material is limited and when analysis is performed in a single attempt. Using the most representative and inclusive CV_A value for calculating the RCV is crucial for making informed decisions about the significance of observed

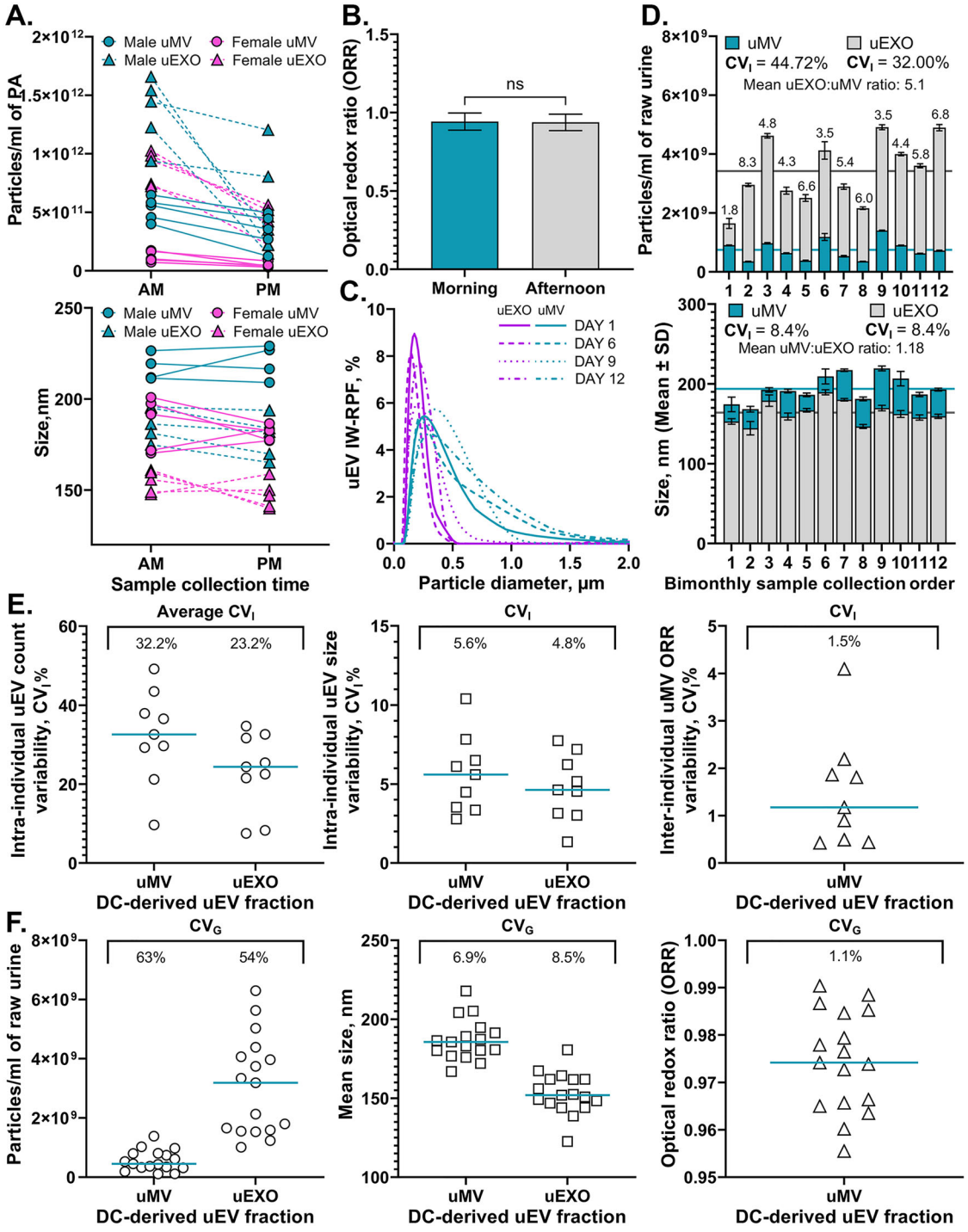

FIGURE 10 | Biological variability of biophysical urinary extracellular vesicle (uEV) characteristics following uEV isolation by differential velocity centrifugation (DC) method. (A) The robustness of short-term (within-day) diurnal variations in uEV particle concentration (upper panel) and size (bottom panel). Morning (6–9 AM) or afternoon (12–2 PM) urine was collected five times from the same male (teal symbols) or female (pink symbols) individuals over 1-month interval. Particle concentration was measured in sequentially isolated microvesicle (uMV, *circle symbols*) or exosome (uEXO, *triangle symbols*) fractions by nanoparticle tracking analysis (NTA) technique. (B) The absence of significant diurnal variations in optical redox ratio values of uMV particles. (C) Representative intermediate-term (between-day) intra-individual variations in uEV particle size. Morning urine was collected from the same male individual over 2-week interval. Intensity-weighted (IW) uMV (*teal lines*) and uEXO (*magenta lines*) particle size distribution was measured by dynamic light scattering (DLS) technique. (D) Representative long-term (bimonthly) intra-individual variations in uEV particle counts and size. Morning urine was collected from the same male individual over two year period. Particle concentration (upper panel) and mean number-weighted size (bottom panel) were co-measured in sequentially isolated uMV (*teal bars*) or uEXO *(grey bars*) fractions by NTA using identical or remarkably close instrumental data acquisition and data analysis settings, including the analyte concentration range. Errors indicate SD of six technical replicate measurements per biological sample. Numbers above bars indicate the uEXO:uMV or uMV:uEXO ratio for particle concentration

(expressed as particles/mL raw urine) or mean size (in nm) measurands, respectively. (E) Intra-individual variability of uEV particle concentration, size and metabolic activity. First morning urine collected from different mixed gender individuals ($N = 7$) at least three independent times was used to measure within-subject coefficient of variation (CV_I) in uEV particle counts (left panel), mean size (middle panel) and ORR (right panel). The horizontal teal line represents the median of data group. (F) Inter-individual variability of uEV particle concentration, size and metabolic activity. First morning urine collected from different mixed gender individuals ($N = 17$) was used to isolate uEVs by the DC method. Concentration (left panel), mean size (middle panel) and ORR (right panel) of indicated uEV fraction particles were measured by either NTA or SLAM microscopy techniques. The horizontal teal line represents the median of data group. The degree of between-subject variations is expressed as CV_G percentage.

differences between two test conditions. To address this unmet need, we investigated the peri-analytical sources of variance attainable to chemically unprocessed, pristine, and fresh (non-frozen) biological human urine sample analysis, and presented the first comprehensive technical report evaluating both biological variability and analytical precision of urine-derived EV (uEV) enumeration, sizing and metabolic status measurements.

Our NTA data provided evidence that traditional 'gold-standard' DC technique that incorporates ultracentrifugation, generates uEV particles exhibiting minimal concentration and size variations across multiple technical replicates (TRs) of the same urine sample, unexpectedly outperforming novel, more rapid and thus increasingly popular uEV isolation methods relying on particle precipitation by solid matrixes such as SiC or PEG.

As illustrated by Sikaris (2008), measurement uncertainty may greatly depend on the number of repeated data points. According to the International Organization for Standardization (ISO) guidelines for standard method performance requirements, test's accuracy and measurement precision should be assessed with a minimum, desired or optimal *replicate sample size* of 5, 7 or 12, respectively, albeit this is a subject of heavy debates, as some strategies suggest using at least 20 replicates for enhanced validity (Serdar et al. 2021). The choice of these arbitrary numbers is often a balance between obtaining meaningful statistical results and the practical considerations of conducting experiments. Researchers and practitioners may sometimes deviate from these recommended values based on specific circumstances and the nature of their experiments. For example, due to the limited space within the swinging-bucket rotor used in this study, only six TRs were analyzed each time to estimate uEV isolation repeatability by DC method. Although our additional fixed-angle rotor had 12 spaces, the working volume of the tubes fitting that rotor was sub-optimal (12 mL), and uEV collection from such tubes was problematic because of the weaker adherence of more spread uEV pellet to the side of the wall following the removal of uEV-depleted supernatant. Manipulation of the centralised pellet in a tube that fitted a swinging-bucket rotor was easier and more reliable. As for the PEG- and SiC-based uEV isolation methods, the number of TRs generated per each independent test-retest experiment ranged between 8 and 12, which offered a more robust evaluation of precision due to more refined central tendency and uncertainty of consecutive measurement results. Unlike in the case of chemically stable standard reference samples, conducting within-day experiments with more than 12 naturally occurring EV samples is not practical, because, with time, sample aggregation could introduce a significant measurement bias.

This study is among the first to employ VCA in the uEV research field, providing novel insights into the sources of variability affecting basic uEV property measurements. It highlights that procedural processing variations of source sample contribute most significantly to the overall variability of DC-derived uEV concentration measurements by NTA, whereas random instrumental variations are the largest in uEV size measurements by both NTA and DLS techniques. By contrast, there is no single dominant source of variation in uMV ORR assessment by SLAM microscopy, which offered a unique advantage of the direct, rapid and extremely precise ($CV_A = 0.7\%$) real-time quantitative measurement of metabolic processes within EVs at single-particle resolution without altering their natural state (Boppart et al. 2019). A combination of DC and NTA or DC and SLAM methods met at least the optimal method's performance goal ($CV_A < 0.5 \times CV_I$, Table 3) further improved by applying subsample pooling strategy. The detailed methodological description of our experimental conditions enables any future data validation by inter-laboratory reproducibility studies if they use similar materials, equipment, and concentration range of final analytes (FAs).

To the best of our knowledge, only one study aimed at comparing the repeatability of biofluid-derived EV isolation by distinct methods (DC, SEC and asymmetric depth-filtration (ADF)) while properly disclosing all instrumental EV concentration and size measurement settings for both NTA and DLS techniques (Chernyshev et al. 2022). In test-retest precision experiments by Chernyshev et al., one of biological samples was split into five aliquots (TRs). Following primary analyte (PA) unfreezing, isolated plasma-derived EV count, size and mode of each TR was measured over a single NTA run (5 RMs with CT = 60 s) or five DLS runs (12 RMs). The PPF number in a diluted FA used for the NTA ranged between 30 and 50, and data was analyzed at DT = 4. According to their results, DC did not demonstrate the highest repeatability among the three methods for particle counting by NTA ($CV_{TR} = 16.5\%$ DC vs. 22.5% SEC vs. 6.7% ADF) but produced the least variable EV number normalized to total protein concentration ($CV_{TR} = 4.1\%$ DC vs. 4.7% SEC vs. 22.7% ADF) (Chernyshev et al. 2022). DC appeared to be the least repeatable when assessing the uniformity of mean particle size ($CV_{TR} = 8.9\%$ DC vs. 8.3% SEC vs. 4.1% ADF) or modal size ($CV_{TR} = 12.7\%$ DC vs. 8.7% SEC vs. 8.1% ADF). In our study, the imprecision of particle counting and sizing in comparable DC-derived uEXO fraction was much lower ($CV_{TR} = 6.1\%$ and 2.15%, respectively).

Tiruvayipati et al. assessed the variability of protein cargo detection in both biological and technical replicates of human lung adenocarcinoma cell EVs (Tiruvayipati et al. 2020). Particles were isolated from three different cell lines at three different passages by PEG method, and each EV lysate was further divided into three TRs. Passage-related biological replicates showed more variability

than TRs, and it was concluded that their combined analysis contributed to generating a more complete EV protein profile. The authors acknowledged the potential influence of technical factors such as sample extraction, digestion, instrumental variance, and instrumental stability on protein identification by LC/MS analysis but did not quantitate the uncertainty of their EV isolation method (Tiruvayipati et al. 2020).

The instrumental data read precision (CV_{RR}) of naturally occurring EV sample measurements by identical NTA NS300 instrument was assessed by Bachurski et al., who demonstrated serum-derived EV counting repeatability ranging between 9.0% (MV) and 10.1% (EXO) (Bachurski et al. 2019). The modal size evaluation precision in corresponding particle fractions was 6.2% and 3.3%. Bachurski et al. estimated CV_{RR} from three RR measurements (each RR consisted of five 1-min long RM videos) (Bachurski et al. 2019). In our study, repeatability of uEV concentration measurements by NTA was higher, with CV_{RR} = 3.2% for uMV and 2.8% for uEXO particles. The CV_{RR} of respective uEV fraction mean size measurements were 1.7% and 0.85%. It is not excluded that the observed differences in these numbers may be attributed to different sample origin and operator performance or experience.

Our difficulty in finding additional studies focused on evaluation of peri-analytical precision may stem from the fact that terms like reproducibility, repeatability, reliability, efficacy, accuracy, bias, (im)precision, and uncertainty are often used interchangeably or incorrectly, despite their distinct and specific but frequently nuanced meanings. For example, the study by Caradec et al. (2014), which aimed to estimate the reproducibility and efficiency of serum-derived EV extraction methods (as stated in the article's title), compared sucrose cushion density-gradient ultracentrifugation and PEG-based EXO isolation methods. The study used two biological samples but employed different amounts of serum and then measured the appropriately diluted samples using NTA with three recordings (presumably, RRs) for each sample, later stating that the batch process of the software was used to integrate the three technical measurements of each sample (presumably, RMs). Only from a description of statistical analysis (a linear regression test), it became clear that the study, in fact, assessed linearity and compared how well the response of each method (EV enumeration and protein concentration) aligned with changes in primary analyte concentration over a specified range. Unfortunately, this is not an isolated singular instance highlighting the potential for confusion when terminology is not correctly or consistently applied. In attempt to alleviate the situation, we provided a glossary of definitions for the metrological terms, as well as introduced a suggested classification of samples (Table S1) and measurements (Table S2) for EV-oriented metrological studies (see Supplementary Material).

We also assessed the biological inter-individual (CV_G) and intra-individual (CV_I) variations of uEV concentration, size and for the first time, the uEV-associated ORR values in healthy human volunteers. Cancer cells often exhibit distinct metabolic profiles, and changes in the ORR can provide unique insights into their metabolic reprogramming, which leads to increased glycolysis (the Warburg effect) and elevated NAD(P)H levels relative to FAD. This shift in the redox balance may result from the higher energy demands and rapid proliferation of cancer stroma cells (Alhallak et al. 2016, Gandhi and Das 2019). Thus, the uEVs of suspected cancer patient may exhibit a decreased ORR compared to healthy individual's uEVs, indicating an enhanced reducing environment within the developing primary or secondary tumor cells. In addition, change in metabolism is an early marker of drug response in cells, and its measurement in uEVs could be an appealing and conceivably sensitive way to assess the early (un)favorable patient response to the applied anti-cancer therapy.

Our findings of relatively high CV_I for excreted uEV numbers and, to a much lesser extent, uEV size and ORR even within a relatively short period of time, underline the following recommendation: to evaluate reliably the baseline level, cutoff value and potential risk status of a specific individual based on uEV-related measurands, the urine should be collected repeatedly at a specified time interval and time of the day. The obtained biological samples should be processed by the most consistent uEV isolation method employing at least multiple sub-samples (TRs) or even sub-sub-samples (FAs) that may eventually be pooled and then repetitively examined by a chosen instrumentation to eliminate the impact of influential procedural sample processing and sample draw errors. Comparison of pooled sample data and the arithmetic mean of TRs demonstrates high concordance in uMV and uEXO particle measurements. This recommendation supports and extends the current MISEV2023 guidelines that primarily address the biological sample pooling requirements (Welsh et al. 2024).

So far, each medical laboratory must determine its own RIs for all analytes in use on the basis of at least 120 healthy individuals by way of the 2.5 and 97.5 percentiles or must at least check existing information on the basis of 20 healthy controls using data mining tools (Hoffmann et al. 2016; Katayev et al. 2015; Obstfeld et al. 2021). Because of the limited healthy participant enrollment number and relatively short follow-up time, we could not determine more reliable RI stratified by fixed age, race/ethnicity, BMI and gender factors. Nevertheless, the evaluation of combined analytical precision (CV_A) allowed us to compute preliminary clinically meaningful IOI and RI indices, which have not been previously reported for these specific uEV analytes and measurands. The closest comparable study that used a similar experimental design to determine the inter-individual, intra-individual, technical and instrumental variations, albeit on a different set of measurands and using a different combination of uEV isolation and detection techniques, was conducted by Oeyen et al. (2019). Specifically, Oeyen et al. extracted uEVs using ultrafiltration and SEC methods to estimate CV_I, CV_G as well as CV_A parameters (CV_{TR} + CV_{RR}) for uEV protein and lipid measurements by MS (Oeyen et al. 2019). Notably, CV_{RR} was calculated by analysing the same sample six times ($m = 6$), whereas procedural sample processing variations were established by using six TRs ($k = 6$) generated by splitting the urine of one individual. To estimate CV_I, Oeyen et al. collected six urine samples from one individual ($N = 1$) at different time points, whereas in our study, a minimum of three independent biological specimen collections from seven individuals ($N = 7$) was used. Additionally, the longitudinal stability of uEV-associated protein patterns (but not particle number or size) within and between individuals was investigated by Erozenci et al. (2021).

The importance of between-subject and within-subject variability in circulating small size EV abundance, morphological characteristics and cargo when performing biomarker analyzes was emphasized by Newman et al. (2021). Like in our study, they used a small cohort of healthy participants ($N = 10$, mean age = 29) and employed NTA technique for EV analysis (five 60 s RM videos were captured and analyzed under constant sample flow conditions (SPS = 50)). However, the EVs used in Newman et al. study originated from serum and were isolated by a different multi-step method (SEC followed by particle concentration via 30 kDa Amicon Ultra-4 centrifuge filters) (Newman et al. 2021). Besides, the aliquoted PA samples were stored at −80°C until analyzed or processed further, whereas we analyzed fresh PAs. Although the precision of serum EV isolation method was not explicitly investigated by Newman et al., the variations in EV concentration as well as modal size measurements between 5 male and 5 female participants were assessed under non-fasting or fasting conditions at different time of blood sampling (AM—morning and PM—afternoon). Since the authors provided only the range, but not the arithmetic mean of NTA values, we requested raw data for manual calculation of CV_G. In this way, serum-derived EV particle count and size data was made more comparable to our study. According to our calculations, the mean ± SE of serum EV number in 10 people irrespective of fasting or time of sampling was $4.25 \times 10^{11} \pm 1.14 \times 10^{11}$ with an estimated $CV_G = 85.0\%$, which was larger than that of uEVs examined in this study (54%–63%). When stratified based on gender, male CV_G was markedly lower than female CV_G (35.8% vs. 75.7%). When EV counts were averaged across PM and AM for both fasting and non-fasting conditions, the mean EV concentration in males was 5.54-fold higher than in females ($p = 0.0014$). Irrespective of fasting conditions, male samples collected at AM hours contained 1.42-fold more EVs compared to PM samples, but this difference was insignificant. A similar trend was observed in our study—more uEVs were found in AM compared to PM samples and male AM urine tended to contain more particles than female AM urine. In Newman et al. study, the mean size of morning serum EVs in non-fasting male and female individuals was 109 nm with SD = 13 nm, and resultant CV_G of 12.2%. Irrespective of fasting status, the CV_G for mean size of serum-derived EVs was 10.9% (AM), 8.1% (PM) or 8.2% (irrespective of sample collection time). These values were comparable to the CV_G of uEXO particles investigated in this study (6.9% to 8.5%).

5 | Limitations of the Study

In this study, peri-analytical precision (CV_A) was estimated for only a limited number of uEV isolation strategies, excluding other well-established and widely adopted EV separation techniques such as SEC, (immune)affinity capture, (ultra)filtration, flow cytometry and others. These methods may produce high purity uEVs but have limited throughput or involve higher costs and longer processing times. Following the presented workflow, CV_A can similarly be evaluated for these methods and/or their combinations. Besides, it is known that precision can vary across the analytical range of an assay, but the evaluation of CV_A in our experiments was performed at a single moderate freshly isolated uEV analyte concentration range. Depending on the sample type, each repeatability assessment round took 1.5–3 h per one experimental condition. Thus, the comparison of precision at higher, mid-range and lower concentration end of the same analyte may take up too much time increasing the risk of uEV aggregation.

The source of outliers in EV isolation and analysis process deserves a separate topic, but inconsistencies may occur due to batch-to-batch variations of chemical reagents and plasticware, pipetting errors, carryover of reagents affecting downstream analysis, instrumental drift, focus shifts in single-particle analyzer, air bubble formation during NTA, EV aggregation, and so forth. The occurrence rate of outliers should be evaluated in a separate study using chemically stable artificial nanoparticles. The users should be aware that even though there are several methods suitable for the detection of outliers, currently, there are no firmly established guidelines how to deal with them within original unmodified NTA datasets.

Next, our CV_A results were reported as average short-term intra-laboratory precision, even though we conducted multiple test-retest experiments on different days. As mentioned earlier, intermediate precision is typically assessed on identical or similar samples, but the measurements are conducted under slightly varied conditions over an extended time, which involve different days, different batches/lots of reagents, and minor changes in environmental conditions. While our collected data met these criteria, the assessment of day-to-day consistency of repeatability estimates for each separate uEV isolation method should be interpreted with caution, because the extent of variability observed among independent analyte isolation and measurement events might be attributed to the inherent characteristics of the biological sample. Ideally, a proper evaluation of intermediate precision should be conducted on uEVs isolated from multiple TRs of urine taken from the *same* person. Unfortunately, EVs are not that stable and will change with time even upon −80°C storage (Gelibter et al. 2022). While this approach is feasible, it necessitates a resolute and sustained commitment to follow-up experiments and is not always practical. Additionally, what if one individual's particles are by default more uniform and render better repeatability?

Due to the sensitive nature of uEV samples, data was collected by a single experienced operator, thus intra-laboratory reproducibility (operator-to-operator agreement) studies should be established separately in future studies. Moreover, the repeatability of EV isolation using the DC method should be evaluated for other sub-populations of uEVs. In this study, the 12 and 100K pellet suspensions were subjectively designated as uMV and uEXO fractions, respectively, despite a significant size overlap of nanoparticles between them. We assure that a small size subpopulation of uEVs remaining in the SN of the 100K fraction (referred to as uEXO2) can be successfully isolated by additional ultracentrifugation round at 120K for up to 16 h; however, the concentration of uEXO2 particles appears to be lesser than that of uEXO fraction (data not shown).

Finally, biological variability was assessed in a limited cohort of healthy participants under only partially standardised conditions (morning samples with fasting status unknown). Intriguingly, some gender-based differences in uEV isolation consistency were observed, however, further studies involving a larger number of male and female subjects are needed to confirm their significance

and identify the underlying causes. THP is known to entrap uEVs, but reportedly, there are no substantial sex-dependent differences in THP excretion rate and concentration in morning spot urine (Eitan et al. 2017). Therefore, it is unlikely that lower particle concentration measurement precision in uEVs isolated from healthy female urine TR samples compared to male TR samples could be attributed to uneven baseline THP levels. On the other hand, potential sex-related differences in polymerised THP filament aggregation rates *ex vivo* cannot be totally excluded. Furthermore, we noticed that BCA assay that was employed to evaluate the total protein concentration among six raw urine TRs subsequently subjected to the DC process in six individuals already resulted in quite sizeable variation (CV = 12.4%, data not shown). While it does not necessarily point to differing starting uEV material in the sub-samples, this observation supports the need for careful source sample handling techniques. At this point, we did not aim to test how the addition of PBS or chemical agents that reportedly enhance the recovery of uEVs, by either lowering the viscosity of the fluid (Momen-Heravi et al. 2012) or by disrupting the THP fibers (Fernandez-Llama et al. 2010; Musante et al. 2012; Correll et al. 2022; Liu et al. 2018; Gheinani et al. 2018; Rood et al. 2010) affected the repeatability of uEV isolation. We also chose not to use any chemical additives due to their unknown effects and potential direct impact on the functional metabolic status of uEVs. Additional experiments may need to be performed to determine whether the magnitude of sample processing errors (CV_{TR}) positively correlates with the delay time in processing both fresh and frozen archived biological samples, and whether urine pre-clearance by filtration or its supplementation with protease inhibitors or other chemical reagents affects the repeatability of uEV isolation. In addition, size distribution measurements may be impacted by uEV recovery yield, which has not been assessed in this study.

EV concentration reflects the balance between particle secretion and internalisation rate, which could be readily impacted by age, race/ethnic background, gender, diet, and physical activity status of participants. For example, after adjusting for BMI, plasma EV concentration decreases with advancing human age, although total EV protein amount in individual subjects does not significantly change over time (Pruijm et al. 2016). Overall, there is limited information available regarding how specific diet and fluid intake impact the abundance and compositional heterogeneity of uEVs in both short- and long-term contexts. To represent physiological conditions more accurately, the participants of this study were not given specific instructions to fast or alter their dietary habits before providing random urinary specimen. Liquid biopsy-based uEV profiling along with meticulous dietary intake diary would be needed to assess the impact of meals and their frequency to the determination of more accurate CV_I in the future studies.

Most common clinical chemistry reference range databases do not yet list CV_G, CV_I or CV_A estimates of uEV sizing, counting and ORR property assessment procedures. Therefore, our RI and IOI results could not be compared with the pre-existing values. In fact, the Task Force on Global Reference Interval Database regularly meets to discuss the establishment of harmonised tool for global users to upload data and calculate RIs using various statistical methods. In spite of the current barriers of uEV use in clinical analysis addressed by Gonzales et al. (2009), perhaps this database is going to be a home for a newly populated list of biofluid-derived EV properties in the nearest future.

6 | Conclusions

Precision is a key evaluation criterion of technical performance of distinct assays/methods. In this study, we demonstrated that:

1. uEV separation by DC was more repeatable that uEV extraction by PEG or SiC-mediated precipitation methods.
2. Overall short-term intra-laboratory precision of uEV concentration measurements by NTA after uEV separation by DC, was markedly better in larger (uMV) than in smaller (uEXO) particles (~5.5% vs. 9.6%). By contrast, the repeatability of sizing was nearly twice as good in uEXO than in uMV samples (~1.1% vs. 2.0%).
3. Procedural variations had the most influence on both uEXO and uMV counting precision, whereas instrumental (run-to-run) measurement variations were more impactful in uEXO and uMV particle sizing by both NTA and DLS techniques. Sample draw variations tended to occur as systematic error in uEV metabolic indicator (ORR) measurements.
4. uEV-associated protein concentration measurement repeatability varied depending on the uEV fraction type, origin and antigen of interest.
5. Source sample processing and extracted EV sample draw have the potential to introduce the differences and affect the final test results of basic uEV characteristics. Therefore, TR and FA pooling is a suitable strategy to improve short-term precision of uEV property measurements by different downstream techniques.
6. In opposite to ORR measurements by SLAM microscopy, the analytical errors of uEV counting and sizing by NTA are markedly lower than natural biological variations.

Defining the peri-analytical precision is an important step for ensuring the reliability of analytical measurements in laboratory practice dealing with relatively new but rapidly expanding diagnostic and prognostic EV biomarker research field. This metrological study can serve as a foundation and a practical guideline for assessing biological and analytical variability and reporting more robust and inclusive CV_A values, both within and across laboratories.

Author Contributions

Edita Aksamitiene: Conceptualization(Equal), Data curation(Equal), Formal analysis(Lead), Investigation(Equal), Methodology(Lead), Validation(Equal), Visualization(Lead), Writing - original draft(Equal). **Jaena Park**: Conceptualization(Supporting), Data curation(Equal), Formal analysis(Equal), Investigation(Equal), Methodology(Supporting), Validation(Equal), Visualization(Supporting), Writing - original draft(Equal). **Marina Marjanovic**: Project administration(Lead), Resources(Supporting), Supervision(Lead), Writing - review & editing(Supporting). **Stephen A. Boppart**: Conceptualization(Equal), Data curation(Lead), Funding

acquisition(Lead), Project administration(Lead), Resources(Lead), Validation(Lead), Supervision(Lead), Writing - review & editing(Lead).

Acknowledgements

The authors thank Darold Spillman, Jr., MA, for his administrative business, information technology and resource management support. We are also grateful to the former and current University of Illinois Urbana-Champaign Microscopy Suite staff, namely Drs. Leilei Yin, Joshua C. Gibson and Catherine L. Wallace for providing methodological training and technical support for the NTA, DLS and TEM instruments. We also thank Prof. Marni Boppart for sharing the ChemiDoc MP Imaging System.

Conflicts of Interest

The authors declare no conflicts of interest.

Data Availability Statement

De-identified data available on request from the authors and through a collaborative research agreement.

References

Aksamitiene, E., J. B. Hoek, B. Kholodenko, and A. Kiyatkin. 2007. "Multistrip Western Blotting to Increase Quantitative Data Output." *Electrophoresis* 28, no. 18: 3163–3173.

Alhallak, K., L. G. Rebello, T. J. Muldoon, K. P. Quinn, and N. Rajaram. 2016. "Optical Redox Ratio Identifies Metastatic Potential-Dependent Changes in Breast Cancer Cell Metabolism." *Biomedical Optics Express* 7, no. 11: 4364–4374.

Analytical Methods Committee Amctb N. 2015. "An Analyst's Guide to Precision." *Analytical Methods* 7, no. 20: 8508–8510.

Bachurski, D., M. Schuldner, P. H. Nguyen, et al. 2019. "Extracellular Vesicle Measurements With Nanoparticle Tracking Analysis—An Accuracy and Repeatability Comparison Between NanoSight NS300 and ZetaView." *Journal of Extracellular Vesicles* 8, no. 1: 1596016.

Benedikter, B. J., F. G. Bouwman, T. Vajen, et al. 2017. "Ultrafiltration Combined With Size Exclusion Chromatography Efficiently Isolates Extracellular Vesicles From Cell Culture Media for Compositional and Functional Studies." *Scientific Reports* 7, no. 1: 15297.

Boppart, S. A., S. You, L. Li, J. Chen, and H. Tu. 2019. "Simultaneous Label-Free Autofluorescence-Multiharmonic Microscopy and Beyond." *APL Photonics* 4, no. 10: 100901.

Bosch, S., L. de Beaurepaire, M. Allard, et al. 2016. "Trehalose prevents aggregation of exosomes and cryodamage." *Scientific Reports* 6: 36162.

Braga, F., and M. Panteghini. 2016. "Generation of Data on Within-Subject Biological Variation in Laboratory Medicine: An Update." *Critical Reviews in Clinical Laboratory Sciences* 53, no. 5: 313–325.

Caradec, J., G. Kharmate, E. Hosseini-Beheshti, H. Adomat, M. Gleave, and E. Guns. 2014. "Reproducibility and Efficiency of Serum-Derived Exosome Extraction Methods." *Clinical Biochemistry* 47, no. 13-14: 1286–1292.

Chernyshev, V. S., R. N. Chuprov-Netochin, E. Tsydenzhapova, et al. 2022. "Asymmetric Depth-Filtration: A Versatile and Scalable Method for High-Yield Isolation of Extracellular Vesicles With Low Contamination." *Journal of Extracellular Vesicles* 11, no. 8: e12256.

Clos-Garcia, M., A. Loizaga-Iriarte, P. Zuniga-Garcia, et al. 2018. "Metabolic Alterations in Urine Extracellular Vesicles Are Associated to Prostate Cancer Pathogenesis and Progression." *Journal of Extracellular Vesicles* 7, no. 1: 1470442.

Comfort, N., K. Cai, T. R. Bloomquist, M. D. Strait, A. W. Ferrante, Jr, and A. A. Baccarelli. 2021. "Nanoparticle Tracking Analysis for the Quantification and Size Determination of Extracellular Vesicles." *Journal of Visualized Experiments* 169. https://doi.org/10.3791/62447.

Correll, V. L., J. J. Otto, C. M. Risi, et al. 2022. "Optimization of Small Extracellular Vesicle Isolation From Expressed Prostatic Secretions in Urine for In-Depth Proteomic Analysis." *Journal of Extracellular Vesicles* 11, no. 2: e12184.

Coskun, A., S. Sandberg, I. Unsal, et al. 2021. "Personalized Reference Intervals in Laboratory Medicine: A New Model Based on Within-Subject Biological Variation." *Clinical Chemistry* 67, no. 2: 374–384.

Eitan, E., J. Green, M. Bodogai, et al. 2017. "Age-Related Changes in Plasma Extracellular Vesicle Characteristics and Internalization by Leukocytes." *Scientific Reports* 7, no. 1: 1342.

Erdbrugger, U., C. J. Blijdorp, I. V. Bijnsdorp, et al. 2021. "Urinary Extracellular Vesicles: A Position Paper by the Urine Task Force of the International Society for Extracellular Vesicles." *Journal of Extracellular Vesicles* 10, no. 7: e12093.

Erozenci, L. A., S. R. Piersma, T. V. Pham, I. V. Bijnsdorp, and C. R. Jimenez. 2021. "Longitudinal Stability of Urinary Extracellular Vesicle Protein Patterns Within and Between Individuals." *Scientific Reports* 11, no. 1: 15629.

Fernandez-Llama, P., S. Khositseth, P. A. Gonzales, R. A. Star, T. Pisitkun, and M. A. Knepper. 2010. "Tamm-Horsfall Protein and Urinary Exosome Isolation." *Kidney International* 77, no. 8: 736–742.

Fey, D., E. Aksamitiene, A. Kiyatkin, and B. N. Kholodenko. 2017. "Modeling of Receptor Tyrosine Kinase Signaling: Computational and Experimental Protocols." *Methods in Molecular Biology* 1636: 417–453.

Fraser, C. G., and E. K. Harris. 1989. "Generation and Application of Data on Biological Variation in Clinical Chemistry." *Critical Reviews in Clinical Laboratory Sciences* 27, no. 5: 409–437.

Gandhi, N., and G. M. Das. 2019. "Metabolic Reprogramming in Breast Cancer and Its Therapeutic Implications." *Cells* 8, no. 2: 89.

Gao, J., A. Li, J. Hu, L. Feng, L. Liu, and Z. Shen. 2022. "Recent Developments in Isolating Methods for Exosomes." *Frontiers in Bioengineering and Biotechnology* 10: 1100892.

Gelibter, S., G. Marostica, A. Mandelli, et al. 2022. "The Impact of Storage on Extracellular Vesicles: A Systematic Study." *Journal of Extracellular Vesicles* 11, no. 2: e12162.

Gheinani, A. H., M. Vogeli, U. Baumgartner, et al. 2018. "Improved Isolation Strategies to Increase the Yield and Purity of Human Urinary Exosomes for Biomarker Discovery." *Scientific Reports* 8, no. 1: 3945.

Gonzales, P. A., T. Pisitkun, J. D. Hoffert, et al. 2009. "Large-Scale Proteomics and Phosphoproteomics of Urinary Exosomes." *Journal of the American Society of Nephrology* 20, no. 2: 363–379.

Görgens, A., G. Corso, D. W. Hagey, et al. 2022. "Identification of Storage Conditions Stabilizing Extracellular Vesicles Preparations." *Journal of Extracellular Vesicles* 11, no. 6: e12238.

Gupta, S., S. Rawat, V. Arora, et al. 2018. "An Improvised One-Step Sucrose Cushion Ultracentrifugation Method for Exosome Isolation From Culture Supernatants of Mesenchymal Stem Cells." *Stem Cell Research & Therapy* 9, no. 1: 180.

Haj-Ahmad, Y. 2018. "Methods for Extracellular Vesicle Isolation and Selective Removal." In: *US10160964B2*. NorgenBiotek Corp.

Hoffmann, G., R. Lichtinghagen, and W. Wosniok. 2016. "Simple Estimation of Reference Intervals From Routine Laboratory Data." *LaboratoriumsMedizin* 39, no. s1.

Jones, G., and A. Barker. 2008. "Reference Intervals." *Supplement, Clinical Biochemist Reviews* 29, no. S1: S93–S97.

Kalluri, R., and K. M. McAndrews. 2023. "The Role of Extracellular Vesicles in Cancer." *Cell* 186, no. 8: 1610–1626.

Katayev, A., J. K. Fleming, D. Luo, A. H. Fisher, and T. M. Sharp. 2015. "Reference Intervals Data Mining: No Longer a Probability Paper Method." *American Journal of Clinical Pathology* 143, no. 1: 134–142.

Kowal, E. J. K., D. Ter-Ovanesyan, A. Regev, and G. M. Church. 2017. "Extracellular Vesicle Isolation and Analysis by Western Blotting." *Methods in Molecular Biology* 1660: 143–152.

Kurian, T. K., S. Banik, D. Gopal, S. Chakrabarti, and N. Mazumder. 2021. "Elucidating Methods for Isolation and Quantification of Exosomes: A Review." *Molecular Biotechnology* 63, no. 4: 249–266.

Lai, J. J., Z. L. Chau, S. Y. Chen, et al. 2022. "Exosome Processing and Characterization Approaches for Research and Technology Development." *Advanced Science (Weinh)* 9, no. 15: e2103222.

Lee, J., E. Kim, J. Park, S. Choi, M. S. Lee, and J. Park. 2023. "Pre-Analytical Handling Conditions and Protein Marker Recovery From Urine Extracellular Vesicles for Bladder Cancer Diagnosis." *PLOS ONE* 18, no. 9: e0291198.

Lee, N., A. Canagasingham, M. Bajaj, et al. 2022. "Urine Exosomes as Biomarkers in Bladder Cancer Diagnosis and Prognosis: From Functional Roles to Clinical Significance." *Frontiers in Oncology* 12: 1019391.

Lee, Y., S. EL Andaloussi, and M. J. A. Wood. 2012. "Exosomes and Microvesicles: Extracellular Vesicles for Genetic Information Transfer and Gene Therapy." *Human Molecular Genetics* 21, no. R1: R125–R134.

Lim, S. Y., J. I. Jang, H. Yoon, and H. M. Kim. 2022. "Spectroscopic Study of Time-Varying Optical Redox Ratio in NADH/FAD Solution." *Journal of Physical Chemistry B* 126, no. 47: 9840–9849.

Liu, W. Z., Z. J. Ma, and X. W. Kang. 2022. "Current Status and Outlook of Advances in Exosome Isolation." *Analytical and Bioanalytical Chemistry* 414, no. 24: 7123–7141.

Liu, Z., D. M. Cauvi, E. M. A. Bernardino, et al. 2018. "Isolation and Characterization of Human Urine Extracellular Vesicles." *Cell Stress & Chaperones* 23, no. 5: 943–953.

Livshits, M. A., E. Khomyakova, E. G. Evtushenko, et al. 2015. "Isolation of Exosomes by Differential Centrifugation: Theoretical Analysis of a Commonly Used Protocol." *Scientific Reports* 5: 17319.

Lone, S. N., S. Nisar, T. Masoodi, et al. 2022. "Liquid Biopsy: A Step Closer to Transform Diagnosis, Prognosis and Future of Cancer Treatments." *Molecular Cancer* 21, no. 1: 79.

McAlinden, C., J. Khadka, and K. Pesudovs. 2015. "Precision (repeatability and reproducibility) Studies and Sample-Size Calculation." *Journal of Cataract & Refractive Surgery* 41, no. 12: 2598–2604.

Momen-Heravi, F., L. Balaj, S. Alian, et al. 2012. "Impact of Biofluid Viscosity on Size and Sedimentation Efficiency of the Isolated Microvesicles." *Frontiers in Physiology* 3: 162.

Musante, L., M. Saraswat, E. Duriez, et al. 2012. "Biochemical and Physical Characterisation of Urinary Nanovesicles Following CHAPS Treatment." *PLOS ONE* 7, no. 7: e37279.

Musante, L., M. Saraswat, A. Ravida, B. Byrne, and H. Holthofer. 2013. "Recovery of Urinary Nanovesicles From Ultracentrifugation Supernatants." *Nephrology, Dialysis, Transplantation* 28, no. 6: 1425–1433.

Musante, L., D. Tataruch-Weinert, D. Kerjaschki, M. Henry, P. Meleady, and H. Holthofer. 2017. "Residual Urinary Extracellular Vesicles in Ultracentrifugation Supernatants After Hydrostatic Filtration Dialysis Enrichment." *Journal of Extracellular Vesicles* 6, no. 1: 1267896.

Newman, L. A., A. Fahmy, M. J. Sorich, O. G. Best, A. Rowland, and Z. Useckaite. 2021. "Importance of Between and Within Subject Variability in Extracellular Vesicle Abundance and Cargo When Performing Biomarker Analyses." *Cells* 10, no. 3: 485.

Obstfeld, A. E., K. Patel, J. C. Boyd, et al. 2021. "Data Mining Approaches to Reference Interval Studies." *Clinical Chemistry* 67, no. 9: 1175–1181.

Oeyen, E., H. Willems, R. 'T Kindt, et al. 2019. "Determination of Variability Due to Biological and Technical Variation in Urinary Extracellular Vesicles as a Crucial Step in Biomarker Discovery Studies." *Journal of Extracellular Vesicles* 8, no. 1: 1676035.

Palacios-Ferrer, J. L., M. B. García-Ortega, M. Gallardo-Gómez, et al. 2021. "Metabolomic Profile of Cancer Stem Cell-Derived Exosomes From Patients With Malignant Melanoma." *Molecular Oncology* 15, no. 2: 407–428.

Park, J., R. L. Kamerer, M. Marjanovic, et al. 2022. "Label-Free Optical Redox Ratio From Urinary Extracellular Vesicles as a Screening Biomarker for Bladder Cancer." *American Journal of Cancer Research* 12, no. 5: 2068–2083.

Petersen, P. H., C. G. Fraser, S. Sandberg, and H. Goldschmidt. 1999. "The Index of Individuality Is Often a Misinterpreted Quantity Characteristic." *Clinical Chemistry and Laboratory Medicine* 37, no. 6: 655–661.

Plant, A., and R. Hanisch. 2020. "Reproducibility in Science: A Metrology Perspective." *Harvard Data Science Review* 2, no. 4.

Pruijm, M., B. Ponte, D. Ackermann, et al. 2016. "Associations of Urinary Uromodulin With Clinical Characteristics and Markers of Tubular Function in the General Population." *Clinical Journal of the American Society of Nephrology* 11, no. 1: 70–80.

Quinn, K. P., G. V. Sridharan, R. S. Hayden, D. L. Kaplan, K. Lee, and I. Georgakoudi. 2013. "Quantitative Metabolic Imaging Using Endogenous Fluorescence to Detect Stem Cell Differentiation." *Scientific Reports* 3: 3432.

Rood, I. M., J. K. Deegens, M. L. Merchant, et al. 2010. "Comparison of Three Methods for Isolation of Urinary Microvesicles to Identify Biomarkers of Nephrotic Syndrome." *Kidney International* 78, no. 8: 810–816.

Royo, F., P. Zuniga-Garcia, V. Torrano, et al. 2016. "Transcriptomic Profiling of Urine Extracellular Vesicles Reveals Alterations of CDH3 in Prostate Cancer." *Oncotarget* 7, no. 6: 6835–6846.

Sanderson, M. J., I. Smith, I. Parker, and M. D. Bootman. 2014. "Fluorescence Microscopy." *Cold Spring Harbor Protocols* 2014, no. 10: pdb top071795.

Schork, N. 2022. "Accommodating Serial Correlation and Sequential Design Elements in Personalized Studies and Aggregated Personalized Studies." *Harvard Data Science Review* Special Issue, no. 3.

Serdar, C. C., M. Cihan, D. Yucel, and M. A. Serdar. 2021. "Sample Size, Power and Effect Size Revisited: Simplified and Practical Approaches in Pre-Clinical, Clinical and Laboratory Studies." *Biochemia Medica (Zagreb)* 31, no. 1: 010502.

Sidhom, K., P. O. Obi, and A. Saleem. 2020. "A Review of Exosomal Isolation Methods: Is Size Exclusion Chromatography the Best Option?" *International Journal of Molecular Sciences* 21, no. 18: 6466.

Sikaris, K. 2008. "Analytical Quality–What Should We be Aiming for?" *Supplement, Clinical Biochemist Reviews* 29, no. S1: S5–S10.

Singh, A. D., S. Patnam, A. Manocha, L. Bashyam, A. K. Rengan, and M. V. Sasidhar. 2023. "Polyethylene Glycol-Based Isolation of Urinary Extracellular Vesicles, an Easily Adoptable Protocol." *MethodsX* 11: 102310.

Sithiravel, C., R. Roysland, B. Alaour, et al. 2022. "Biological Variation, Reference Change Values and Index of Individuality of GDF-15." *Clinical Chemistry and Laboratory Medicine* 60, no. 4: 593–596.

Sohal, I. S., and A. L. Kasinski. 2023. "Emerging Diversity in Extracellular Vesicles and Their Roles in Cancer." *Frontiers in Oncology* 13: 1167717.

Sorrells, J. E., J. Park, E. Aksamitiene, et al. 2024. "Label-Free Nonlinear Optical Signatures of Extracellular Vesicles in Liquid and Tissue Biopsies of Human Breast Cancer." *Scientific Reports* 14, no. 1: 5528.

Stankovic, A. K., and E. DiLauri. 2008. "Quality Improvements in the Preanalytical Phase: Focus on Urine Specimen Workflow." *Clinics in Laboratory Medicine* 28, no. 2: 339–350. viii.

Tangwattanachuleeporn, M., P. Muanwien, Y. Teethaisong, and P. Somparn. 2022. "Optimizing Concentration of Polyethelene Glycol for Exosome Isolation From Plasma for Downstream Application." *Medicina (Kaunas, Lithuania)* 58, no. 11: 1600.

Taylor, S. C., L. K. Rosselli-Murai, B. Crobeddu, and I. Plante. 2022. "A Critical Path to Producing High Quality, Reproducible Data From Quantitative Western Blot Experiments." *Scientific Reports* 12, no. 1: 17599.

Tepus, M., E. Tonoli, and E. A. M. Verderio. 2022. "Molecular Profiling of Urinary Extracellular Vesicles in Chronic Kidney Disease and Renal Fibrosis." *Frontiers in Pharmacology* 13: 1041327.

Testa, A., E. Venturelli, and M. F. Brizzi. 2021. "Extracellular Vesicles: New Tools for Early Diagnosis of Breast and Genitourinary Cancers." *International Journal of Molecular Sciences* 22, no. 16: 8430.

Thomas, C. E., W. Sexton, K. Benson, R. Sutphen, and J. Koomen. 2010. "Urine Collection and Processing for Protein Biomarker Discovery and Quantification." *Cancer Epidemiology and Prevention Biomarkers* 19, no. 4: 953–959.

Tiruvayipati, S., D. Wolfgeher, M. Yue, et al. 2020. "Variability in Protein Cargo Detection in Technical and Biological Replicates of Exosome-Enriched Extracellular Vesicles." *PLOS ONE* 15, no. 3: e0228871.

Walton, R. M. 2012. "Subject-Based Reference Values: Biological Variation, Individuality, and Reference Change Values." *Veterinary Clinical Pathology* 41, no. 2: 175–181.

Weigelin, B., G. J. Bakker, and P. Friedl. 2016. "Third Harmonic Generation Microscopy of Cells and Tissue Organization." *Journal of Cell Science* 129, no. 2: 245–255.

Welsh, J. A., D. C. I. Goberdhan, L. O'Driscoll, et al. 2024. "Minimal Information for Studies of Extracellular Vesicles (MISEV2023): From Basic to Advanced Approaches." *Journal of Extracellular Vesicles* 13, no. 2: e12404.

World Medical Association. 2013. "World Medical Association Declaration of Helsinki: Ethical Principles for Medical Research Involving Human Subjects." *JAMA* 310, no. 20: 2191–2194.

Xu, R., D. W. Greening, H. J. Zhu, N. Takahashi, and R. J. Simpson. 2016. "Extracellular Vesicle Isolation and Characterization: Toward Clinical Application." *Journal of Clinical Investigation* 126, no. 4: 1152–1162.

Yakubovich, E. I., A. G. Polischouk, and V. I. Evtushenko. 2022. "Principles and Problems of Exosome Isolation From Biological Fluids." *Biochemistry (Moscow) Supplement. Series A, Membrane and Cell Biology* 16, no. 2: 115–126.

Yang, Q., J. Luo, H. Xu, et al. 2023. "Metabolomic Investigation of Urinary Extracellular Vesicles for Early Detection and Screening of Lung Cancer." *Journal of Nanobiotechnology* 21, no. 1: 153.

You, S., H. Tu, E. J. Chaney, et al. 2018. "Intravital Imaging by Simultaneous Label-Free Autofluorescence-Multiharmonic Microscopy." *Nature Communications* 9, no. 1: 2125.

Yu, D., Y. Li, M. Wang, et al. 2022. "Exosomes as a New Frontier of Cancer Liquid Biopsy." *Molecular Cancer* 21, no. 1: 56.

Supporting Information

Additional supporting information can be found online in the Supporting Information section.